Exploring the Temporal-Varying and Depth-Nonlinear Velocity Profile of Debris Flows Based on A Stratification Statistical Algorithm for 3D-HBP-SPH Particles

Zheng HAN[1], Wendou Xie[2], Chuicheng Zeng[1], Yange Li[1], Changli Li[1], Haohui Ding[1], Weidong Wang[1], Ningsheng Chen[3], Guisheng Hu[4], and Guangqi Chen[5]

[1]Central South University
[2]CSU
[3]Institute of Mountain Hazards and Environment, C.A.S.
[4]Chinese Academy of Sciences,Key Laboratory of Mountain Hazards and Surface Process, Institute of Mountain Hazards and Environment
[5]Kyushu University

April 16, 2023

Abstract

Estimation of velocity profile through mud depth is a long-standing and essential problem in debris-flow dynamics. Until now, various velocity profiles have been proposed based on the regression of experimental measurements, but these are often limited by the observation conditions, such as the number of the configured sensors. Therefore, the resulting linear velocity profiles exhibit limitations in reproducing the nonlinear behavior and its temporal variation during the debris-flow process. In this study, we present a novel approach to explore debris-flow velocity profile in detail upon our previous 3D-HBP-SPH numerical model, i.e., the three-dimensional Smoothed Particle Hydrodynamic model incorporating with the Herschel-Bulkley-Papanastasiou rheology. Specifically, we propose a stratification statistical algorithm for interpreting the details of SPH particles, which enables the recording of temporal velocities of debris flow at different mud depths. To regress the velocity profile, we introduce a logarithmic-based nonlinear function with two empirical parameters, that controlling the shape of velocity profile and concerning its temporal evolution. We verify the proposed velocity profile and explore its sensitivity using 34 sets of velocity data from three individual flume experiments in previous literatures. Our results demonstrate that the proposed temporal-varying and depth-nonlinear velocity profile outperforms the previous ones.

Hosted file

Exploring the Temporal-Varying and Depth-Nonlinear Velocity Profile of Debris Flows Based on A Stratification Statistical Algorithm for 3D-HBP-SPH Particles

Zheng HAN[1,2], Wendou XIE[1], Chuicheng ZENG[1], Yange LI[1,3*], Changli LI[1], Haohui DING[1], Weidong WANG[1], Ningsheng CHEN[4], Guisheng HU[4], Guangqi CHEN[5]

[1] School of Civil Engineering, Central South University, Changsha 410075, China.

[2] Hunan Provincial Key Laboratory for Disaster Prevention and Mitigation of Rail Transit Engineering Structures, Changsha 410075, China.

[3] The Key Laboratory of Engineering Structures of Heavy Haul Railway, Ministry of Education, Changsha 410075, China.

[4] Key Lab of Mountain Hazards and Surface Processes, Institute of Mountain Hazards and Environment, Chinese Academy of Sciences, Chengdu 610041, China.

[5] Department of Civil Engineering, Kyushu University, Fukuoka, 819-0395, Japan.

Corresponding author: Y. Li (liyange@csu.edu.cn), No.22 Shaoshan South Road, School of Civil Engineering, Central South University, Changsha, Hunan, China. Tel.: +86 18684982076.

Key Points:

- A stratification statistical algorithm for interpreting the dynamics of 3D-HBP-SPH particles is introduced.
- A logarithmic-based model for the temporal-varying and depth-nonlinear velocity profile is regressed.
- 34 sets of velocity data measured in different flume experiments are used to verify the proposed model.

Abstract

Estimation of velocity profile through mud depth is a long-standing and essential problem in debris-flow dynamics. Until now, various velocity profiles have been proposed based on the regression of experimental measurements, but these are often limited by the observation conditions, such as the number of the configured sensors. Therefore, the resulting linear velocity profiles exhibit limitations in reproducing the nonlinear behavior and its temporal variation during the debris-flow process. In this study, we present a novel approach to explore debris-flow velocity profile in detail upon our previous 3D-HBP-SPH numerical model, i.e., the three-dimensional Smoothed Particle Hydrodynamic model incorporating with the Herschel-Bulkley-Papanastasiou rheology. Specifically, we propose a stratification statistical algorithm for interpreting the details of SPH particles, which enables the recording of temporal velocities of debris flow at different mud depths. To regress the velocity profile, we introduce a logarithmic-based nonlinear function with two empirical parameters, that a controlling the shape of velocity profile and b concerning its temporal evolution. We verify the proposed velocity profile and explore its sensitivity using 34 sets of velocity data from three individual flume experiments in previous literatures. Our results demonstrate that the proposed temporal-varying and depth-nonlinear velocity profile outperforms the previous ones.

Plain Language Summary

Studies of debris-flow dynamics involves estimating the velocity profile through mud depth. Conventional velocity profiles in previous studies were limited by observation conditions and were unable to reproduce the nonlinear behaviour and its temporal variation. Here, we propose a new approach to explore debris-flow velocity profiles through three-dimensional numerical simulation using the smoothed particle hydrodynamic (SPH) method. A stratification statistical algorithm is introduced to analyse the details of SPH particles based on the numerical results to record and output temporal velocities of debris flow at different mud depths. A logarithmic-based function with two parameters is introduced to regress the nonlinear velocity profile with temporal variation. It is verified using 34 sets of velocity data from three individual flume experiments. The results show that the proposed depth-nonlinear and temporal-varying velocity profile performs better than previous ones.

1 Introduction

Debris flows are highly sediment-laden flows mixing with mud, stones, organic materials, and water, travelling at high velocities in steep channels. This kind of fluid–solid flows pose severe risks to residential societies at the mountainous area, and often cause serious casualties and property losses worldwide each year (Dowling & Santi, 2014; Godt & Coe, 2007; VanDine & Bovis, 2002). Their unpredictable initiation, tremendous destructive power, and long run-out distance represent a challenging task of engineering design and plan for hazard mitigation and prevention. Many catastrophic cases have been reported recent years, for example, the August 8, 2010, Zhouqu debris flow event destroying approximately 5500 buildings in China (Chen et al., 2019; Tang et al., 2011), as well as the 2003 debris flow events at the Faucon region damaging many existed sabo dams in the Swiss Alps (Remaître et al., 2008).

The tremendous destructive power of debris flows can be explained in part by their high travelling velocities. Therefore, predicting on the debris-flow velocity has long been an essential issue on the topic of debris-flow mitigation research. In fact, as a typical two-phase phenomenon, debris-flow velocity distribution is one of the most complex problems in the dynamic mechanism due to the flow's opacity caused by its high concentration of solid particles (Rickenmann, 1999; Han et al., 2015a; Chen et al., 2017). Moreover, inertial collision of the solid particles, coarse grain friction, viscous shear, and interaction between solid and fluid phase during the debris-flow process arise uncertainties and difficulties when estimating its travelling velocities (Du et al., 2021; Iverson, 1997). Therefore, it remains a great scientific challenge to provide an exact solution for describing the complex flowing behavior of debris flows.

In this sense, a common and acceptable solution is to reduce its complexity by representing the debris-flow velocity field into the lateral distribution and the vertical profile through a cross-section. As to the lateral distribution, common wisdom often holds that debris-flow velocity is greater along the thalweg and getting smaller at both sides of the channel (Han et al., 2015a). Many remarkable studies can be referred to, such as the experimental investigation by Iverson et al. (2001) and Tecca et al. (2003), as well as the theoretical solution in our previous study (Han et al., 2014). Also, many numerical models based on the depth-averaged Navier-Stokes equations (e.g., Luna et al. 2012; Ouyang et al., 2015) have been employed to investigate the velocity of debris flow.

Nevertheless, the vertical velocity profile of the debris flow shows more complicated dynamics due to the high concentration and frequent collisions of solid particles. The velocity profile of debris flow relates to its internal deformation, holding essential information on hydrodynamics and flow resistance. Generally, the overall features of the debris-flow velocity profile have been discussed and substantiated in many previous studies, that the velocity at the free surface is much higher than that at the fluid bottom (Johnson et al., 2012). Nagl et al. (2020) summarized four possible types of velocity profile, i.e., constant velocity profile with full basal sliding, flow profile over rigid bed with no basal sliding, combination of basal sliding and internal deformation, and flow over an erodible bed. They mentioned that the vertical velocity profiles are strongly linked to flow characteristics such as pore-fluid pressure, grain size distribution and density variations.

Systematic measurements of velocity profiles in real-scale debris flows are not yet available (Nagl et al., 2020), therefore, flume experiments are an alternative way to investigate the complex phenomenon of debris-flow velocity profile (Wei & Hu, 2009). Many previous studies used measurement devices, such as ultrasonic sensors, radar, or seismic sensors, to obtain the debris flow velocities (e.g., Arattano & Marchi, 2005; Chen et al., 2017; Iverson & Vallance, 2001; Johnson et al., 2012; Nagl et al., 2020; Prochaska et al., 2008; Tecca et al., 2003; Wei et al., 2012). These previous studies well documented the measurement data of vertical velocities and provided an insight into the velocity profile of debris flow. Based on the observed features of vertical velocity distribution, some linear or non-linear velocity profile have been assumed, such as in Hotta and Ohta (2000), Johnson et al. (2012), and Han et al. (2015a). Notably, these established velocity profiles in different studies commonly have a similar form which can be expressed as below,

$$v(z) = f\left(\alpha, \left(\frac{z}{h}\right)^{\beta}\right) \tag{1}$$

where f denotes the velocity profile, z is the vertical location beyond the bed, h is the flow depth. α presents an empirical parameter controlling the amount of shear within the bulk of flow. β denotes an anther parameter controlling linear or nonlinear behavior considering basal slip. However, owing to that in most of the flume experiments, the amount of the velocimeter sensors in the array is limited, difficulties arise when regressing a good-fitting nonlinear profile with such limited amount of measurement data. Also, the best-fitting values of the involved empirical parameters α and β are currently debated among the existing studies. In view of this, the single-parameter linear velocity profiles, and have been applied in many numerical studies (e.g., Ouyang et al., 2015; Han et al., 2015b).

Intense velocity data through the depth definitely benefits a better regression of debris-flow velocity profile. Recently, particle image velocimetry (PIV) has been witnessed a great potential in exploring the dynamics of two-phase flows due to its non-invasive measurement, full-field, instantaneous flow velocity maps (Gabriele et al., 2011; Liu & Lam, 2015). Owing to that direct measurements for opaque debris flows are problematic (Iverson, 2012), therefore, for better observation of tracer particles, high fluid transparency and relatively low solid concentration should be considered. Many studies, e.g., Chen et al. (2017) used mixture of machine oil and white oil to represent the debris flow fluid with a similar viscosity. Regardless of the argument that whether oil-mixture is adequate for representing debris-flow fluid, the PIV-based experimental data demonstrates a more obvious nonlinear velocity profile. Many previous studies, e.g., Chen et al. (2017), Du et al., (2021) and Han et al. (2022), recommended a usage of logarithm-based function to regress the nonlinear velocity profile, which could better fit with the experimental measurements.

However, it should be noticed that velocity profile of debris flows has not yet been well recognized. One key problem is with respect to the temporal variation of the debris-flow velocity profile. In most of the previous experimental studies, capturing the instantaneous velocity at different depths is a tough task. This difficulty commonly lies in the measurement using either the image-based velocimetry of PIV or the ultrasonic sensor-based velocimetry in flume experiments. Meanwhile, uncertainties due to collision of the solid particles bring noises in the measurement data, which are difficult to recognize and denoise. Therefore, mean velocity at different depths during the debris flow process has to be used, which inherently hides the feature of temporal variation.

Besides, the debris-flow event may occur as a single surge or as a sequence of multiple surges (e.g., Arai et al., 2013; Zanuttigh & Lamberti, 2007). Even in a surge, the inhomogeneous debris-flow mass has been observed complex dynamics, that turbulence flow at the debris flow surge front would transit into a laminar one at the surge end when debris flow passes by Pudasaini et al. (2020). As a consequence, the velocity profile varies with the flow status. Evidence could be found in the remarkable real-scale experiment by Nagl et al. (2020), that velocity profiles at the front part, the main body show obvious different shapes. This concept and evidence inspired the subsequent research on how the observed temporal variation could be considered in the regression of debris-flow velocity profile.

In this paper, based on the proposed 3D-HBP-SPH numerical model (Han et al., 2021a), we reproduce the debris-flow flume experiments by Iverson et al. (2011) where debris-flow dynamics were well-documented. We propose a particle-location based stratification statistical algorithm to analyze the temporal velocities at different depth. With the interpreted temporal velocity distribution, a double-parameter, logarithmic-based function is regressed to describe the velocity profile variation with time-elapse. The measurements of velocity data presented in other three previous flume experiment by Egashira et al. (1989), Hotta et al. (1998) and Chen et al. (2017) are used to illustrate the effect of the proposed temporal-varying and depth-nonlinear velocity profile.

2 Methodologies

2.1 The proposed 3D-HBP-SPH numerical model

As mentioned above, a better regression of debris-flow velocity profile depends on a greater amount of velocity data at different depth. Many flume experimental studies used ultrasonic sensors to measure debris-flow velocities. However, due to the size of the sensors, the total number of the sensors are limited, the collected measurement data are insufficient to present the observed nonlinear velocity profile in other PIV-based experiments.

Therefore, in this paper, we use particle-based numerical model to explore the debris-flow velocity profile. In general, this kind of particle-based model provides a 3D description of the debris-flow dynamic process through discrete particles and approximately solves the Navier-Stokes (N-S) equations in discrete form (Hungr & McDougall, 2009; McDougall & Hungr, 2005), so that a large amount of debris-flow dynamic data can be recorded. Considering the complex rheology of debris-flow mass, here we use our previous three-dimensional SPH model based on Herschel-Bulkley-Papanastasiou (HBP) rheology (Han et al., 2019, 2021a), the so-called 3D-HBP-SPH model, the positive effect of which has been substantiated by the following studies (Huang et al., 2022; Morikawa & Asai, 2022; Yu et al., 2020). The details of the model could be referred to Han et al. (2019) and Han et al. (2021a), while the basics of this model is introduced in detail in the supporting information Text S1 along with this paper. With the termination of the numerical simulation using 3D-HBP-SPH model, the debris-flow process is able to be reproduced because the spatial positions (x, y, z) and velocity components $\left(v_x, v_y, v_z\right)$ of SPH particles at different time steps are well-documented and sorted.

2.2 Particle stratification statistical algorithm

It should be noted that a total of approximately 10^5 to 10^6 SPH particles are commonly used to represent debris-flow mass in a three-dimensional simulation, each of these particles shows different spatial positions and velocity vectors. It is inadequate to simply choose some among all the particles for regressing the velocity profile, because the chosen particles could not be able to describe the overall behavior of debris flow. In this sense, all the particles must be comprehensively considered.

These recorded dynamic data in particle form should be processed before they can be further used to demonstrate the debris-flow velocity profile. In this paper, a major contribution is with respect to the particle stratification statistical algorithm, which is specifically designed to analyze the temporal average velocity of the SPH particles at different flow depths. The proposed algorithm is introduced as following.

2.2.1 Coordinate system transformation

The numerical simulation result of the 3D-HBP-SPH model is a time-series dataset, with a time interval Δt. In a certain time step t, the spatial positions (x, y, z) and velocity components (v_X, v_Y, v_Z) of each particle along X, Y, Z directions are included. However, the physical variables of the particles in the SPH scheme are described in absolute coordinates. To better understand the velocity profile, the velocity component (v_X, v_Y, v_Z) of each particle in absolute coordinates should be transformed into the flume bed-linked local coordinate system (X', Y', Z')

(as shown in Figure 1b), so that the velocities along the bed can be conventionally represented by $v_{X'}$. The method for coordinate system transformation is expressed by

$$\begin{bmatrix} x' \\ y' \\ z' \end{bmatrix} = R(\theta_X)R(\theta_Y)R(\theta_Z)\begin{bmatrix} x \\ y \\ z \end{bmatrix} - \begin{bmatrix} x_{origin} \\ y_{origin} \\ z_{origin} \end{bmatrix} \quad (2a)$$

$$\begin{bmatrix} v_X' \\ v_Y' \\ v_Z' \end{bmatrix} = R(\theta_X)R(\theta_Y)R(\theta_Z)\begin{bmatrix} v_X \\ v_Y \\ v_Z \end{bmatrix} \quad (2b)$$

where x_{origin}, y_{origin}, and z_{origin} denotes the origin of the absolute coordinate in the numerical result. $R(\theta_X)$, $R(\theta_Y)$, $R(\theta_Z)$ are the rotation matrixes depending on the inclined angles of the bed along the X, Y, and Z directions, respectively.

$$R(\theta_X) = \begin{bmatrix} cos(\theta_X) & 0 & -sin(\theta_X) \\ 0 & 1 & 0 \\ sin(\theta_X) & 0 & cos(\theta_X) \end{bmatrix} \quad (3a)$$

$$R(\theta_Y) = \begin{bmatrix} 1 & 0 & 0 \\ 0 & cos(\theta_Y) & sin(\theta_Y) \\ 0 & -sin(\theta_Y) & cos(\theta_Y) \end{bmatrix} \quad (3b)$$

$$R(\theta_Z) = \begin{bmatrix} 1 & 0 & 0 \\ 0 & 1 & 0 \\ 0 & 0 & 1 \end{bmatrix} \quad (3c)$$

where θ_X and θ_y are the inclined angles of the bed along X and Y directions. Normally, for the single-section flume, we assume the flume along the X direction. In this case, θ_y equates 0 and $R(\theta_Y) = \begin{bmatrix} 1 & 0 & 0 \\ 0 & 1 & 0 \\ 0 & 0 & 1 \end{bmatrix}$.

2.2.2 Particle recognition in the domain of the cross-section

Velocity profile represents vertical velocity distribution of a selected cross-section. In the numerical simulation results of 3D-HBP-SPH, once a cross-section at $x' = x_0'$ is selected, the particles those passing through this cross-section should be recognized and filtered. However, even though a large number of particles are used in the numerical simulation, the particles those coincidentally passing through the cross-section may be rare. To get a sufficient velocity data for regressing the velocity profile, here as shown in Figure 1c, we expanse the selected cross-section backward and forward for a small distance which we named as the domain length L_{domain}. Thus, the particles with the instantaneous spatial position (x', y', z') that satisfying the criterion $x' \in [x_0' - L_{domain}, x_0' + L_{domain}]$ are supposed within the domain of the selected cross-section, and should be considered in the regression of the velocity profile in this cross-section.

2.2.3 Particles stratification according to their position

Suppose that there are totally n particles in the cross-section domain, with various vertical position z_i' along the Z' direction. The maximum vertical position is $z'_{max} = max(z'_1, z'_2, \cdots z'_n)$ and the minimum one is $z'_{min} = min(z'_1, z'_2, \cdots z'_n)$. Assume a small height Δh pseudo layer, the cross-section domain could be stratified into m layers, that

$$m = \frac{z'_{max} - z'_{min}}{\Delta h} \tag{4}$$

and the vertical location of each layer is

$$H_j = z'_{min} + \Delta h(j-1), (j = 1,2, \cdots, m). \tag{5}$$

Thus, the particles with the vertical position z' that satisfying the criterion $z' \in [H_j, H_{j+1}]$ are supposed belonging to the layer j, and a total number k_j of the particle in each layer j can be counted.

2.2.4 Velocity evaluation of each stratified layer

The above-mentioned algorithm has recognized k_j particles belonging to the layer j. Each particle has velocity components (v'_X, v'_Y, v'_Z) which have been transformed from (v_X, v_Y, v_Z) in the absolute coordinate. Among three velocity components, v'_Y denotes the velocity across the section, v'_Z is the particle velocity through flow depth, while v'_X describes the velocity along the flume. Therefore, as illustrated in Figure 1d, we use the mean value of the velocity component v'_X of each recognized particle to determine the representative velocity of the layer j, which is expressed as

$$\bar{V}_j = \frac{1}{k_j} \sum_{i=1}^{k_j} v'_X(i). \tag{6}$$

where $\bar{V}_j$ is the output velocity of debris flow at the vertical position of $z = H_j$.

The schematic illustration of the proposed particle stratification statistical algorithm is illustrated in Figure 1. In this way, a series of mean velocities $(\bar{V}_1, \bar{V}_2, \cdots, \bar{V}_j)$ at different vertical positions can be obtained and further used for the regression of the velocity profile.

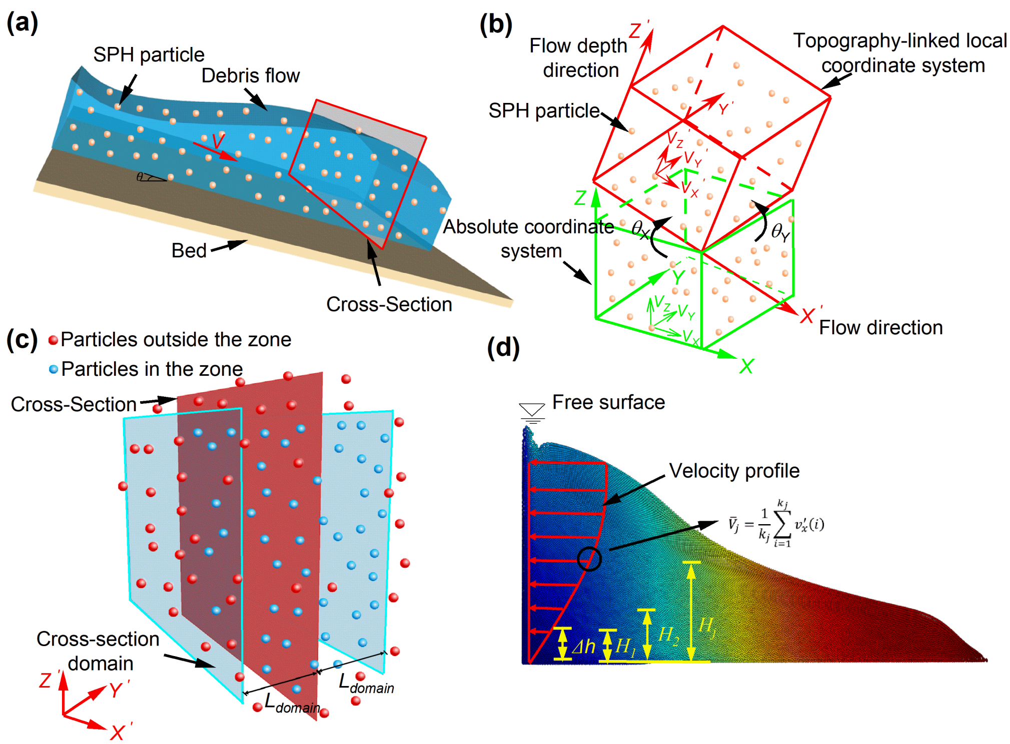

Figure 1. Schematic illustration of the particle hierarchical statistical algorithm. (a) Illustration of the particle-based debris flow process. (b) Coordinate system transformation. (c) Particle recognition in the domain of the cross-section. (d) Particles stratification and velocity evaluation of each stratified layer.

3 Numerical reproduction of the flume experiment

3.1 Numerical simulation of USGS flume test

As we have mentioned above, systematic measurements of velocity profiles in real-scale debris flows are not yet available (Nagl et al., 2020). Therefore, flume experiments with well-documented measurement data become an alternative way, in particular that the flattened flume avoids the influence of complex topography to the debris-flow dynamics in real-scale event. In this paper, we select the USGS flume experiment reported in detail in Iverson et al. (2011) for numerical reproduction. The large-scale flume experiment was designed to explore the positive feedback and momentum growth during debris flow entrainment process and achieved remarkable findings those inspired the following studies. The large-scale flume has a straight concrete channel that 95m in length and 2m in width, inclined at an angle of 31°. As arrays of electronic sensors had been installed in the flume, the dynamics of the experimental debris-flow process, e.g., temporal variation of flow depth, were well-documented and recorded, which could be essential to calibrate the numerical simulation for reproducing this experiment.

This flume experiment has been simulated in our previous study (Han et al., 2022), where a total of 43,258 fluid particles were used to represent the discretized debris-flow mass in the experiment. Nevertheless, in order to better explore the velocity details, more fluid particles are necessary to minimize the uncertainties of particle distribution. In this study, a total of 87,951 fluid particles are generated to discretize the debris-flow mass, which is almost two times more than our previous studies. While 486,694 fixed boundary particles are used to represent the flume structure. As we choose a very small time increment $\Delta t = 0.0001s$ in the numerical simulation, the computational consumption might be high. Therefore, a high-performance computational server, capable of 24 core Intel Xeon Scalable CPU, 2 pieces of NVIDIA Titan V GPU, and 128GB RAM, is employed to execute the numerical computing. Other configurations and values of key parameters are kept the same as we summarized and listed in the previous study (Han et al., 2022).

The debris-flow process that 25s in duration takes almost 48 hours to complete the numerical reproduction. With two-times more particles adopted, the simulation results in Figure 2b show more details for the subsequent exploring of debris flow velocities. To verify the simulation results, the observed positions of debris-flow front in the experiment at different times are used as benchmarks and are compared with the numerical results (as shown in Figure 2c). It is demonstrated that the simulation results are in a good accordance with the observation in the experiment.

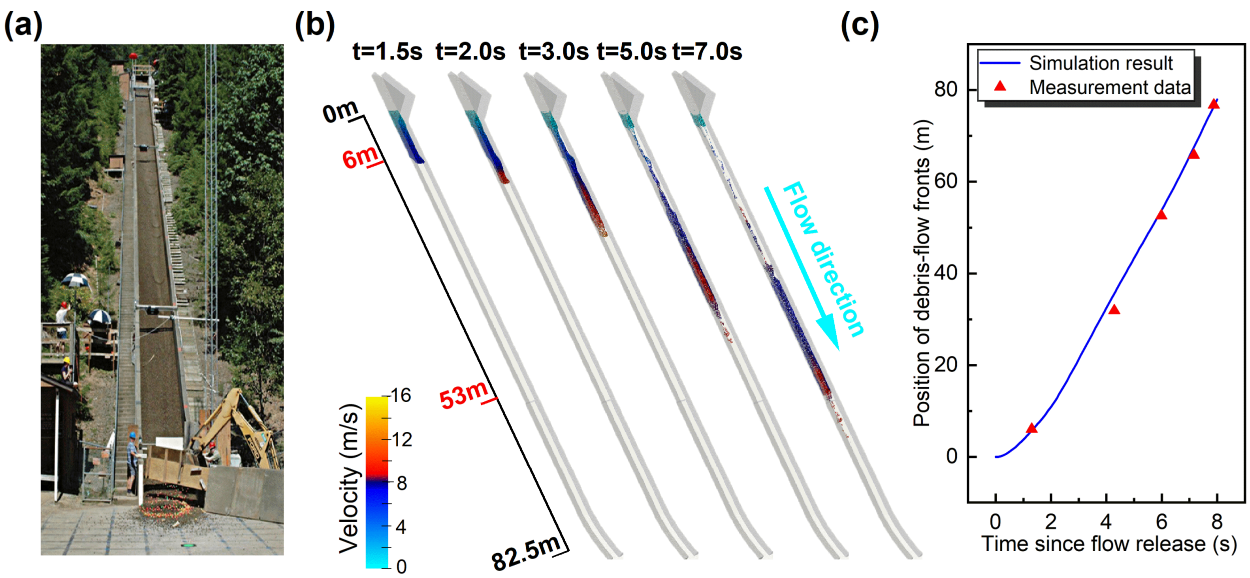

Figure 2. (a) The USGS flume experiment by Iverson et al. (2011). Reproduced from ref. 26 with permission from the Journal of Geophysical Research Earth Surface, copyright 2012. (b) The simulation results of flow velocity. (c) Flow front position at different times.

3.2 Vertical velocity distribution

A cross-section of the flume at the position of $x = 6.0m$ is chosen. We select the cross-section at this position because behind which a 12cm thick tabular layer of sediment had been covered on the bottom of the flume in their experiment, within the range of $x = 6.0m$ and $x = 53.0m$. Combination of basal sliding and internal deformation may arise certainties for exploring velocity profile.

To get a sufficient velocity data, a cross-section domain is generated using $L_{domain} = 0.2m$, which is 5 times the initial particle distance $dp = 0.04m$. As shown in Figure 2c, a single surge of debris flow is observed in the numerical simulation result, coincident with the experiment measurement. Due to that the majority of the debris-flow mass passed through this cross-section during around 1.0s to 5.0s, we choose four different moments, i.e., $t_1 = 1.4s$, $t_2 = 1.6s$, $t_3 = 2.4s$, and $t_4 = 3.2s$, to explore the temporal variation of the vertical velocity distribution, as shown in Figure 3. In Figure 3a, the total number of the particles and flow depth belonging to the selected cross-section is plotted as a function of the simulation time. It is shown that at the four moments, the total number of the particles are all beyond 2000, providing sufficient data to investigate the velocity distributions. Normally, we sperate the cross-section into 11 parallel layers through depth, each of which has around 200 particles with varying velocities v'_X. Subsequently, the mean velocities $\bar{V}_j$ at different vertical position can be calculated and output (as shown in Figure 3b-3e).

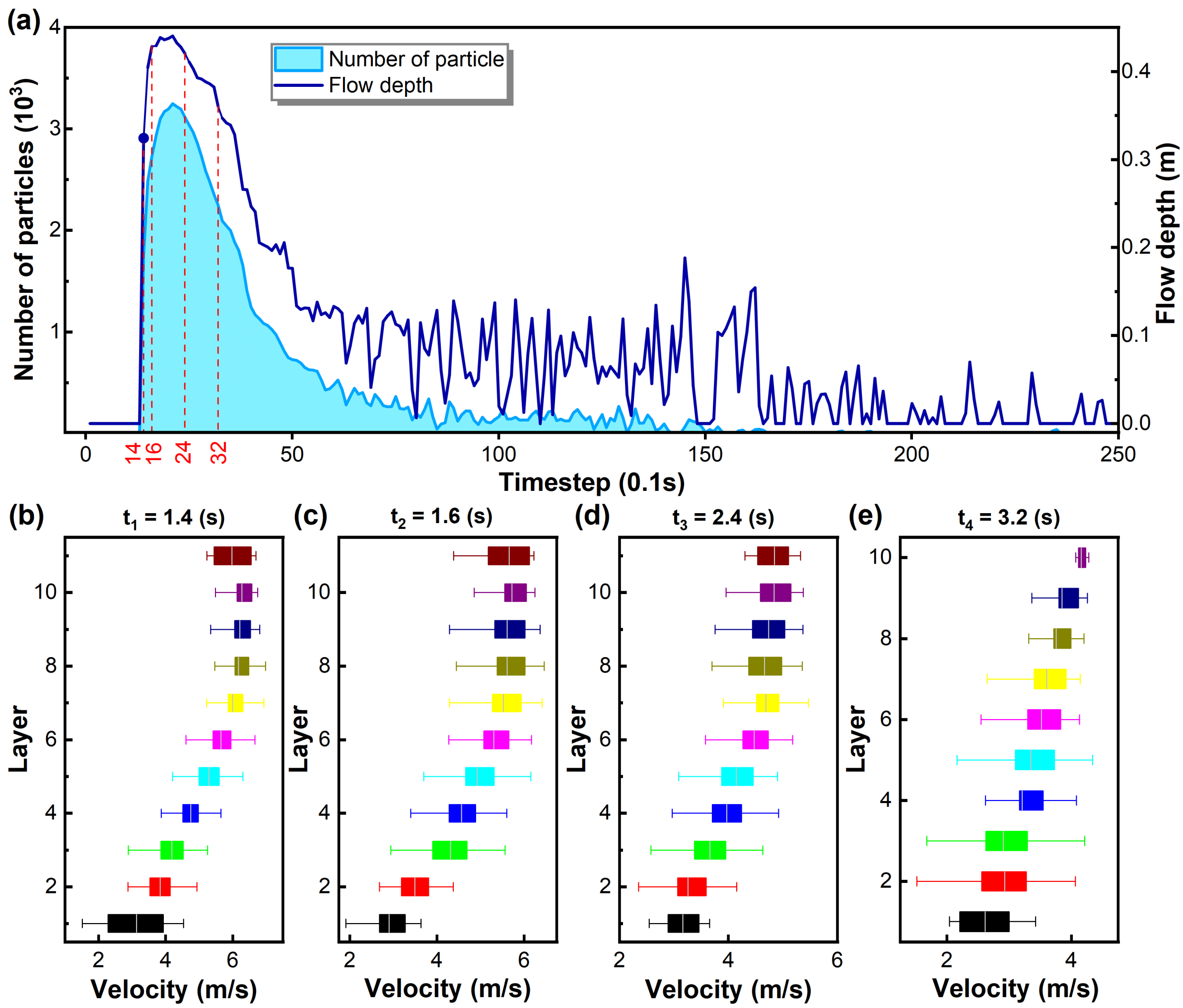

Figure 3. The result of velocity profile in four time-steps. (a) The total number of the particles and flow depth over time. (b) The velocity profile at $t_1 = 1.4s$. (c) The velocity profile at $t_2 = 1.6s$. (d) The velocity profile at $t_3 = 2.4s$. (e) The velocity profile at $t_4 = 3.2s$.

It is shown that at all the four moments, the flow velocity presents a nonlinear distribution through depth. The maximum velocity usually appears at the free surface of the debris flow and gradually reduces through depth. This phenomenon well matches the possible type of velocity profile as mentioned in Nagl et al. (2020) . As to the temporal variation of debris flow velocity, the maximum velocity appears at t_1 and t_2 moments, when the front of debris-flow surge arrives and an approximately 6.0m/s velocity is recorded. The velocity is observed gradually decreasing to around 4.0m/s at the t_4 moment as the majority of debris flow passed, while the division between the top and bottom velocity seems reduced. It may indicate that debris flow transits into approximately a constant one after this moment, the phenomenon of which has also been mentioned in Pudasaini et al. (2020). It should be noticed that at $t_2 = 1.6s$, the velocity at the free surface ($z = 0.35m{\sim}0.40m$) of the main body is slightly smaller, showing a concave-up profile form developed in the main body as observed in the real-scale experiment in Nagl et al. (2020). The observed temporal variation of the vertical distribution of the debris-flow velocity also highlights the necessities to incorporate a time-dependent parameter when regressing the debris-flow velocity profile.

4 Regression of instantaneous velocity profile

4.1 Conventional linear velocity profile

As a comparison, we employ the conventional linear law in the previous studies to regress the velocity profile before we further consider its temporal variation and non-linear features. The function of linear velocity profile is modified from the original one in Johnson et al. (2012) and Iverson (2012) and has been used in our previous studies (Han et al., 2018, 2019). The mathematical expression is

$$V(z) = \bar{V}\left(1 - \alpha + 2\alpha\frac{z}{h}\right) \quad (7)$$

where $V(z)$ denotes the velocity profile as velocity at different vertical positions are known. α is a fitting parameter controlling the amount of shear within the bulk of flow as we mentioned above. It ranges from $\alpha = 0$ if there is no simple shear to $\alpha = 1$ if there is no basal slip. In Johnson et al. (2012), a good fit to experimental measurement was suggested with $\alpha = 0.5$. $\bar{V}$ is the mean velocity of the cross-section at a moment and can be mathematically computed by

$$\bar{V} = \frac{1}{n}\sum_{i=1}^{n} v'_x(i) \quad (8)$$

where n is the total number of the particles belonging to the cross-section domain at a moment.

Given this linear velocity profile, the vertical distribution of the velocities in the numerical results those shown in Figure 3 is regressed. Notice that at each moment, the total number of the particles and their velocities are varying, resulting in different shapes of velocity profile. Therefore, we regress the linear velocity profile every 0.08s and obtain different values of the best fitting parameter α, as shown in Figure 4a. It is obvious that the best fitting values of parameter α varies from 0.2 to approximately 0.8 during the process, with a mean value of 0.45 which is quite approaching the suggested value by Johnson et al. (2012). Notably, the parameter α reduces from $\alpha = 0.8$ at the front of debris-flow surge to $\alpha = 0.2$ at the end of surge, indicating that the main body of the debris flow with internal deformation and shear may evolve into an approximately constant one with no simple shear.

4.2 Nonlinear velocity profile

The vertical velocity profiles as exhibited in Figure 3 indicate an obvious non-linear velocity profile, which has been substantiated in the PIV measurements of a flume experiment by Chen et al. (2017). The nonlinear feature of the velocity profile cannot be well reproduced using the above linear velocity profile. In this sense, a nonlinear velocity profile is necessary to illustrate the complex features of vertical velocity distribution.

In this sub-section, regardless of its temporal variation, we choose a logarithmic-based function to describe the nonlinear velocity profile. To minimize the deviation of debris flow velocity at different moments, we use dimensionless and normalized terms for the regression, which is

$$\frac{V(z)}{V_{max}} = 1 + a \cdot \ln(\frac{z}{h}) \tag{9}$$

where $V(z)/V_{max}$ is the normalized velocity term ranging in $[0,1]$, denoting the ratios of velocities at different vertical positions and the maximum velocity V_{max} in the cross-section. z/h is the normalized vertical position, ranging from $z/h = 0.0$ at the flume bottom to $z/h = 1.0$ at the free surface of the debris flow. a is an empirical-based fitting parameter controlling the complex shape of velocity profile.

Although sometimes a concave-up profile in the main body has been witnessed, it is still problematic to obtain a mathematical expression. Therefore, the regressed nonlinear velocity profile in Eq. (9) ignores concave-up feature and assumes that the maximum velocity appears at the free surface. To demonstrate the effect, two typical moments at $t_1 = 1.4s$ and $t_2 = 1.6s$ is used to illustrate the regression, as shown in Figure 4b and 4c. It is shown that two best fitting values $a = 0.1828$ and $a = 0.1699$ close to each other are obtained, with the satisfactory R-squared values of $R^2 = 0.939$ and $R^2 = 0.965$. We also explored the influence of parameter a on the velocity profile, as shown in Figure 4d. It is demonstrated that with an increasing parameter a, an approximate plug flow ($a < 0.05$) with constant velocity profile evolves into simple shear flow ($a > 0.25$) with internal deformation.

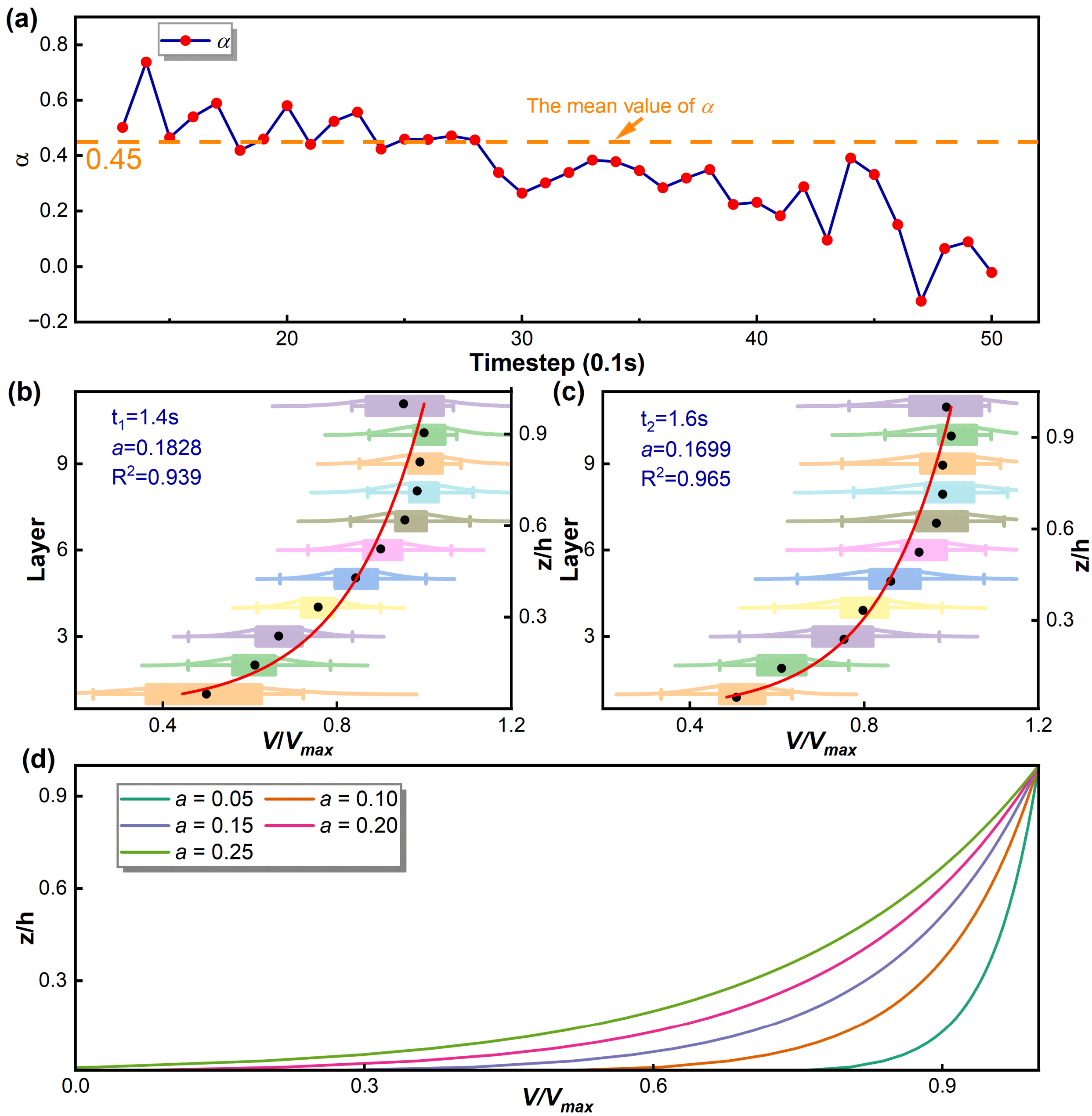

Figure 4. (a) Temporal variation of the best fitting parameter α of the linear velocity profile. (b) Velocity profile fitting regression analysis with $t_1 = 1.4s$. (c) Velocity profile fitting regression analysis with $t_2 = 1.6s$. (d) Analysis of the parameter a of the fitting function.

5 Velocity profile considering temporal variation

5.1 Mathematical expression

As shown in Figure 3, the velocity profiles at four different moments have been witnessed obvious differences in their shape, indicating that the temporal variation of the debris-flow velocity profile should be considered. The abovementioned nonlinear profile only considers its instantaneous shape, therefore, should be improved by incorporating its temporal variation.

For this purpose, we introduce a time-linked parameter b in the logarithmic-based velocity profile in Eq. (10) to describe its temporal variation. The basic form of this temporal-varying, depth-nonlinear velocity profile is express mathematically as below,

$$\frac{V(z)}{V_{max}} = c + a \cdot \ln(\frac{z}{h} + b) \tag{10}$$

Note that a constraint parameter c is temporally introduced in the above equation, because the velocity profile should satisfy a basic assumption that maximum velocity V_{max} should appear at the free surface $z = h$, where the left term of Eq. (10) equates $\frac{V(z)}{V_{max}} = 1.0$. Thus, the constraint parameter c could be reduced to $c = 1 - a \cdot \ln(1 + b)$. In this way, we obtain a dual-parameter velocity profile that describes its temporal-varying, depth-nonlinear features,

$$\frac{V(z)}{V_{max}} = 1 + a \cdot \left[\ln\left(\frac{z}{h} + b\right) - \ln(1 + b)\right] \tag{11}$$

where a is the fitting parameter controlling the complex shape of velocity profile. b is the time-linked parameter controlling the temporal variation of the velocity-profile shape.

Mathematically, the parameter b poses significant influence to the described velocity profile by Eq. (11). To explore its influence in detail, a sensitivity analysis on the parameter b is used, we keep parameter a constant ($a = 0.25$ for simple shear flow is used for instance) but different values of the parameter b ranging from 0.1 to 0.8 are chosen for sensitivity analysis. The resulting velocity profiles are shown in the Figure 5a. It demonstrates that the velocity profile changes gradually from a nonlinear form to a linear one with the increasing value of the parameter b. It should be noticed that the basal velocity of the debris flow increases from $0.4V_{max}$ to $0.8V_{max}$ when the parameter b increase from 0.1 to 0.8. It indicates that a greater value of the parameter b is more adequate for describing the velocity profile of plug flow.

5.2 Time-linked parameter *b* controlling the temporal variation

As we mentioned above, the parameter b is the time-linked parameter controlling the temporal variation of the velocity profile shape, therefore, its values should be highly dependent on the duration of debris-flow process. In this section, we attempt to explore the link between the value of the parameter b and the time t, which is supposed as a mathematical function of $b = f(t)$.

In Section 3, we estimated and documented the velocities at different vertical locations and at different moments in the USGS flume experiment using the proposed 3D-HBP-SPH model. These time-series data provide supports for investigation the details of $b = f(t)$. Because the majority of debris-flow mass passed through the chosen cross-section at $x = 6.0m$ within 5 seconds since debris flow released, we separate the duration between 1~5 second into 50 timesteps, with a time increment of 0.1s. A constant value $a = 0.25$ is used in each timestep, while the best fitting value of the parameter b is obtained. Subsequently, the best fitting values of the parameter b in time-series are plotted as a function of time t, as shown in Figure 5b. It is obvious that the parameter b gradually increases from $b = 0.05$ to $b = 0.30$ with the debris-flow duration. We use a linear function to regress the relation between b and t. The obtained linear function shows a satisfactory R-squared value (>0.90), demonstrating a strong linear relation between b and t.

However, it should be mentioned that the direct usage of the regressed linear function between b and t is limited, because debris-flow duration t significantly varies case by case, even multiple surges are often observed in a single debris-flow event. In this sense, debris-flow duration t is not adequate for directly evaluating the parameter b. Here, we introduce a concept of the normalized time t' in an individual surge to address this issue. For the multi-surge debris flow, each individual surge is separated and then is assumed to follow the triangular hydrograph (Takaoka et al., 2006) as shown in Figure 5c. The single-surge hydrograph has a rising limb, falling limb, and tail limb, wherein three major moments are required to reproduce this hydrograph; t_f represents the moment when debris-flow front arrives the cross-section, t_p represents the debris-flow peak, and t_s represents the moment when debris-flow surge ends. Using this hydrograph, the proposed normalized time t' in an individual surge is expressed as

$$t' = \frac{t - t_f}{t_s - t_f}, t \in [t_f, t_s] \tag{12}$$

In Eq. (12), the term of $t_s - t_f$ denotes the duration of the individual debris-flow surge.

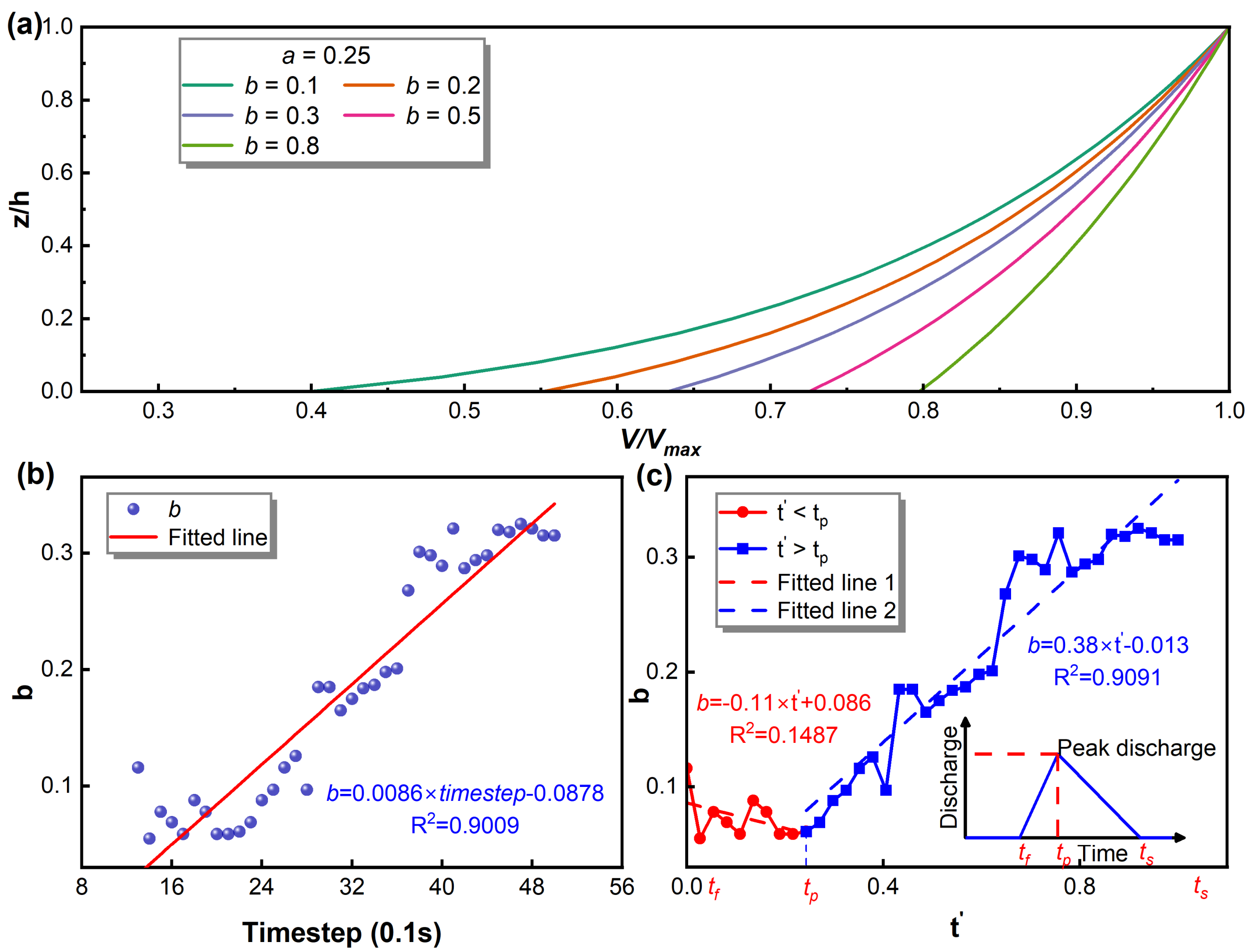

Figure 5. (a) Velocity profile corresponding to different parameter b. (b) The relationship between parameter b and time. (c) The relationship between parameter b and relative time t'.

In this way, the time-series data of the best fitting values for the parameter b can be represented as a function of the normalized time t', as shown in Figure 5c. In accordance with the triangular hydrograph we assumed, the variation of the parameter b shows two obvious stages divided by the peak moment ($t' = 0.21$), as marked in red and blue line in Figure 5c. The red line denotes the time-to-peak stage ($t' \in [0, 0.21]$), when the best fitting value of the parameter b decreases with t'. While the blue line demonstrates the time-after-peak stage ($t' \in [0.21, 1.00]$), in contrast, the best fitting value of the parameter b gradually increases with t'. As indicated in Figure 5c, linear relation between b and t' at both stages are observed, which are regressed as

$$b = \begin{cases} -0.11t' + 0.086, & t' < t_p \\ 0.38t' - 0.013, & t' \geq t_p \end{cases} \tag{13}$$

6 Discussion

As demonstrated in Section 4.2, the proposed velocity profile contains two crucial parameters a and b, which are used to describe the nonlinear characteristics and temporal evolution characteristics of the vertical velocity distribution of debris flow, respectively. In order to better understand the proposed model, we discuss the model sensitivities and verify the model in this section.

6.1 Sensitivity analysis of the parameter a and b

A one-at-a-time sensitivity analysis is performed to assess the impact of input parameters' variation on the improved nonlinear model. All the initial parameters are kept constant except the one chosen for sensitivity analysis. Figure 6 shows the velocity of debris flow as a function of the chosen parameters a and b . As shown in Figure 6, the velocity through the depth decreases with the increase of parameter a but increases as a function of the parameter b. It is indicated that the parameter a shows a more obvious impact compared to a because velocities approaching the bottom ($\frac{z}{h} = 0.1$) vary approximately ±80% when the value of a varies ±100%, it is almost 3.5 times greater compared to the impact of the parameter b. Figure 6 also demonstrates that both two parameters pose more significant influence on the velocities approaching the bottom than the free surface.

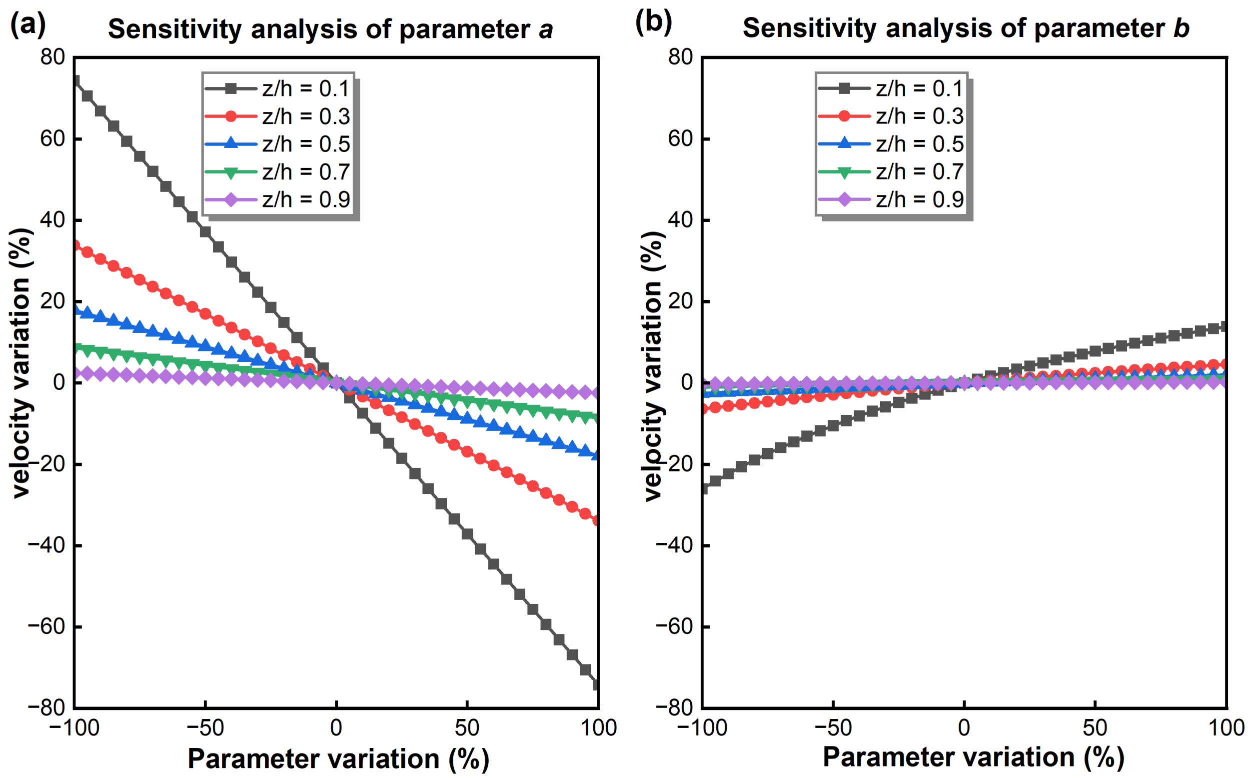

Figure 6. Variation of the resulting in velocities at different vertical location as a function of the parameter a and b. (a) Sensitivity analysis of the parameter a. (b) Sensitivity analysis of the parameter b.

6.2 Verification using velocity measurement data in previous experiments

In order to verify the proposed velocity profile, we use 34 sets of the measured velocity data from three individual flume experiments as reported by Egashira et al. (1989), Hotta et al. (1998), and Chen et al. (2017). The velocity profiles of these experiments are regressed using the proposed model and compared with the existing linear model.

Owing to that the velocity measurement data in three experiments were the mean velocities at the stage approaching to peak, and the details of their temporal variation are not available. Therefore, in this section, a constant mean value of the time-link parameter $b = 0.10$ is pre-defined, owing to that the parameter b ranges from 0.05 to 0.15 at the stage approaching to peak as shown in Figure 5c. In order to evaluate the fitting performance of the proposed model, the residual sum of squares (RSS) is used, which is

$$RSS = \sum_{i=1}^{n} (l_i - v_i)^2 \tag{14}$$

where l_i represents the measured velocity value, v_i represents the velocity estimated by the proposed non-linear profile, and n denotes the number of measured data points in each set of the flume experiment. A smaller value of RSS indicate a better fitting effect.

Results are listed in detail in Table 1, in which Data 1-8 use the flume experiment data by Egashira et al. (1989), Data 9-10 by Hotta et al. (1998), while the remaining by Chen et al. (2017). As a comparison, the previous linear velocity profile as introduced in Eq. (7) is used for comparison, with the suggested values of the fitting parameter α, i.e., $\alpha = 0.25$, $\alpha = 0.50$, and $\alpha = 0.75$, are used respectively (Iverson, 2012; Johnson et al., 2012). It is obvious that the proposed non-linear velocity profile attains better fitting results for 32 sets among all the 34 sets of experiments (The summary of fitting results for 34 sets of experimental data is included in the supporting information Figures S1 to S34, among which 4 groups of data are shown in Figure 7). Results indicate that the proposed velocity profile is more consistent with the experimental data when describing the debris flow velocity.

Table 1. Fitting results of experimental data from Egashira et al. (1989), Hotta et al. (1998) and Chen et al. (2017).

Data id	The proposed non-linear velocity profile		The previous linear velocity profile				
	a	RSS (a)	α	RSS (α)	RSS (α = 0.25)	RSS (α = 0.50)	RSS (α = 0.75)
1	0.3897	0.0713	0.4767	0.2838	0.0216	0.0079	0.0248
2	0.4651	0.2368	0.5270	0.2530	0.0479	0.0102	0.0103
3	0.4745	0.0863	0.6375	0.3295	0.0433	0.0073	0.0096
4	0.5148	0.3158	0.6315	0.5065	0.0566	0.0100	0.0056
5	0.2787	0.1097	0.3046	0.2335	0.0079	0.0184	0.0516
6	0.4529	0.6525	0.3844	0.5122	0.0506	0.0174	0.0193
7	0.3869	0.2844	0.3498	0.2299	0.0210	0.0064	0.0208
8	0.4102	0.1055	0.5022	0.3186	0.0215	0.0070	0.0226
9	0.4378	0.0134	0.8500	0.3052	0.0870	0.0257	0.0166
10	0.4639	0.0350	0.7144	0.2753	0.0762	0.0214	0.0114
11	0.3402	0.0750	0.4902	0.7263	0.0329	0.0170	0.0472
12	0.4452	0.0534	0.8574	3.4257	0.1412	0.0391	0.0132
13	0.3624	0.1053	0.5792	1.0299	0.0547	0.0231	0.0423
14	0.4041	0.3445	0.5418	2.2549	0.0826	0.0356	0.0444
15	0.5288	0.2206	1.1107	2.1595	0.1821	0.0583	0.0132
16	0.3332	0.0590	0.5198	0.7172	0.0391	0.0160	0.0423
17	0.2902	0.0631	0.3680	0.4148	0.0148	0.0174	0.0620
18	0.3730	0.1994	0.7136	2.3323	0.0977	0.0299	0.0301
19	0.4209	0.0373	0.6878	0.8234	0.0681	0.0139	0.0157
20	0.3096	0.0424	0.4275	0.4702	0.0216	0.0103	0.0462
21	0.3437	0.4079	0.4859	2.5437	0.0793	0.0239	0.0358
22	0.3599	0.4702	0.6016	3.9330	0.1131	0.0393	0.0382
23	0.2697	0.0850	0.3281	0.7398	0.0225	0.0268	0.0831
24	0.3445	0.2249	0.5693	2.7017	0.0823	0.0283	0.0428
25	0.3285	0.1180	0.5183	1.0082	0.0461	0.0259	0.0547
26	0.2990	0.1988	0.3739	1.3356	0.0449	0.0296	0.0707
27	0.3872	0.0514	0.6067	3.4303	0.1571	0.0436	0.0082
28	0.3315	0.1120	0.5828	2.3820	0.0708	0.0238	0.0433
29	0.2667	0.0805	0.3140	0.7858	0.0211	0.0256	0.0827

30	0.3649	0.1024	0.5753	0.7953	0.0623	0.0373	0.0554
31	0.2849	0.1200	0.4387	1.2753	0.0439	0.0297	0.0742
32	0.3282	0.2810	0.4569	1.7309	0.0576	0.0334	0.0623
33	0.4143	0.0632	0.8013	4.6371	0.1523	0.0429	0.0177
34	0.3039	0.0451	0.4820	0.6970	0.0354	0.0103	0.0394

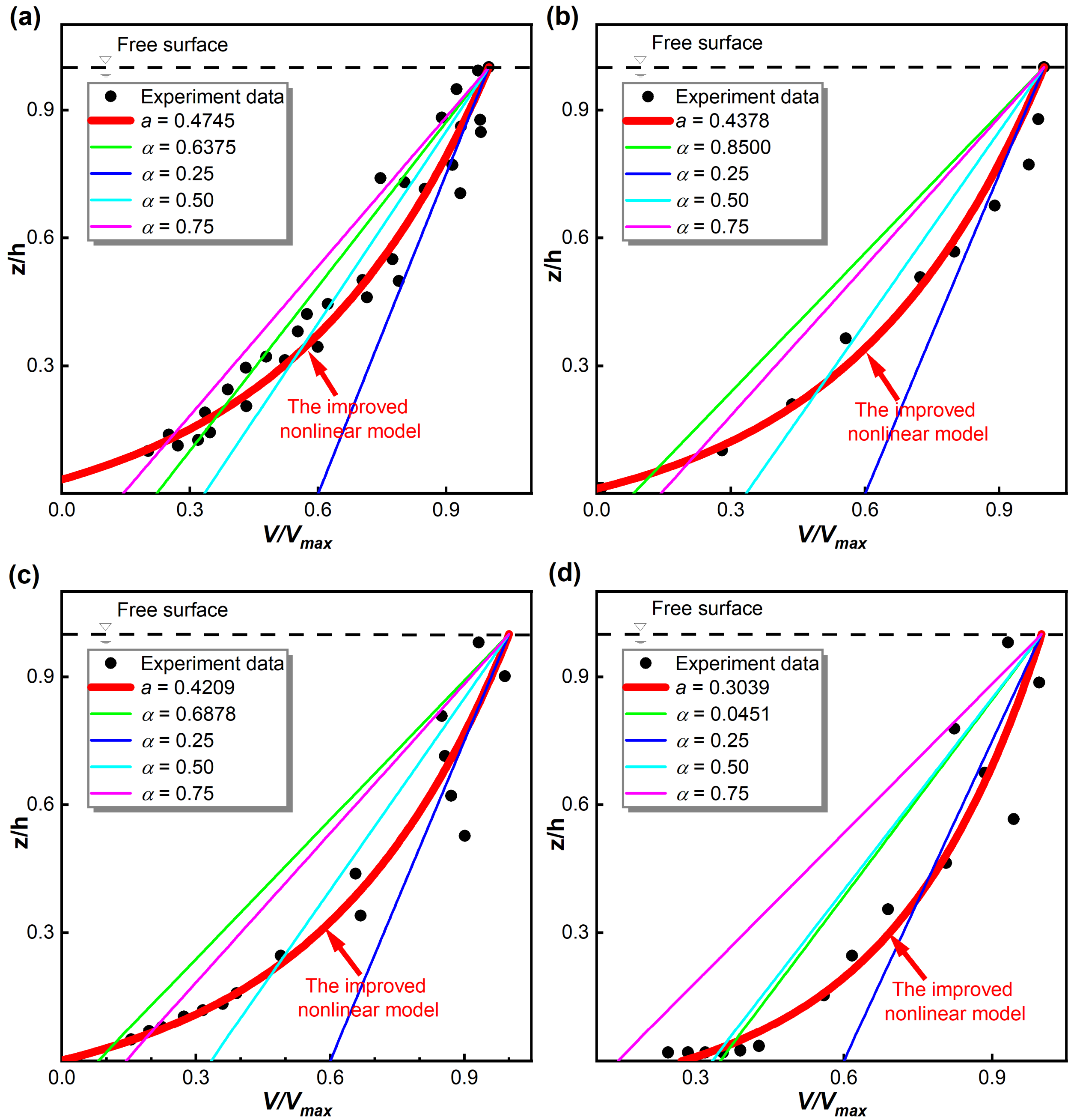

Figure 7. Comparison of the improved nonlinear distribution model and the linear model. (a) Experiment data 3. (b) Experiment data 9. (c) Experiment data 19. (d) Experiment data 34.

6.3 Suggestion for the rational value of the parameters

Sensitivities of the key parameters in proposed profile has been discussed in section 6.1, while in this section, the suggested value and the rational range of the key parameters are discussed, which will be beneficial for practical work. Ideally, a great value range of the parameter may somewhat arise difficulties for practical work if no criteria is provided. This issue has long been highlighted, such as the viscosity coefficient in debris-flow rheology, the rational value of which may vary from a few tens to hundreds of times from measurement (Takahashi, 2009; Han et al., 2017). As to the time-linked parameter b, the expected value could be calculated by Eq. (13) under the assumption of triangular hydrograph. For the cases those excluding the consideration of temporal variation, a rational range of $b \in [0.05, 0.15]$ as shown in Figure 5c could be referred to, with a suggested value of $b = 0.10$ for estimating the mean velocity around the peak.

In contrast, it is more complex to discuss the rational range of the parameter a because this parameter is empirical based. In this section, we provide the suggestion for the rational value of the parameter a based on the above-mentioned verification using 34 sets of experiments. As shown in Figure 8, the median of the best fitting value of the parameter a for all 34 sets of the experiments is 0.3637, while the maximum and the minimum value are 0.5288 and 0.2667, respectively. Figure 8 also demonstrates that half of the best fitting values of the parameter a fall within the range of $[0.3282, 0.4209]$, which is smaller and better comparing to the parameter $\alpha \in [0.4387, 0.6315]$ in conventional linear velocity profile. As such, a rational range of $a \in [0.32, 0.42]$ could be referred to, with a suggested value of $a = 0.36$ for a benchmark for calibration.

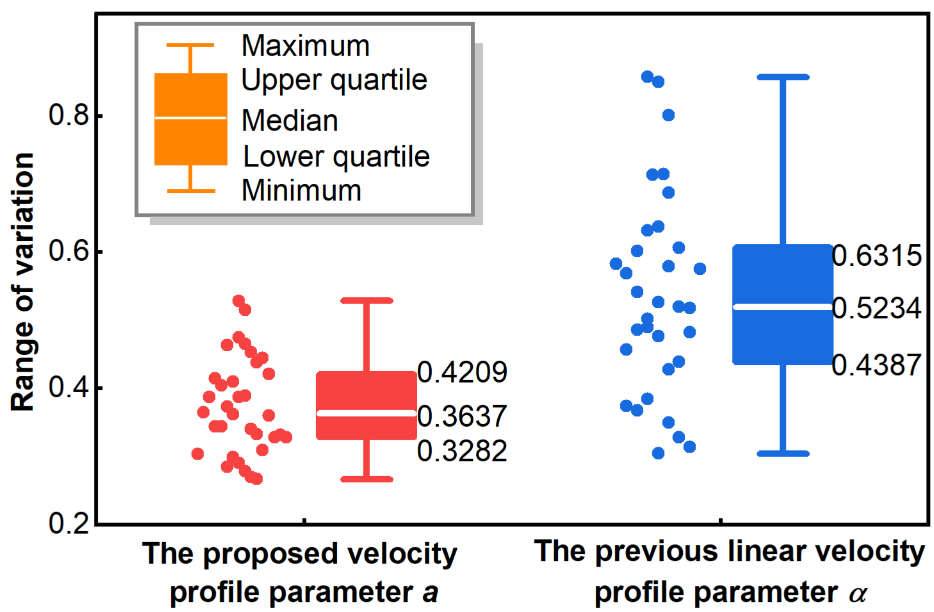

Figure 8. Suggestion and comparison for the rational range of the empirical parameter a and α in the proposed and previous velocity profiles, respectively.

7 Discussion

In this paper, we propose a new approach to explore the temporal-varying and depth-nonlinear velocity profile of debris flows. The debris-flow process is simulated by our previous 3D-HBP-SPH numerical model and recorded in time-series data in particle form. To interpret and analyse the details of debris-flow dynamics, a stratification statistical algorithm that suitable for SPH particles is proposed, upon which the temporal velocities of debris flow at different mud depths during the process could be obtained.

The flume experiments by USGS in the previous study is simulated in order to explore the debris-flow velocity profile. A logarithmic-based nonlinear function is proposed for reproducing the debris-flow velocity profile in detail. The proposed function contains two key parameters, the empirical parameter a controlling the shape of velocity profile, and the time-linked parameter b concerning its temporal evolution. A function connecting the parameter b to the normalized time t' is regressed in particular for the debris flows with the assumed triangular hydrograph.

We verify the proposed velocity profile and explore its sensitivity using 34 sets of velocity data from the three individual flume experiments in previous literatures. Results indicate the rational range of the values for both parameters, wherein $a \in [0.32, 0.42]$ and $b \in [0.05, 0.15]$ are suggested. The conventional linear velocity profiles summarized in previous studies are used for comparison. It is shown that the proposed depth-nonlinear and temporal-varying velocity profile performs better than previous ones.

Acknowledgments

This study was financially supported by the National Natural Science Foundation of China (Grant No. 52078493); the Natural Science Foundation of Hunan Province (Grant No. 2022JJ30700); the Natural Science Foundation for Excellent Young Scholars of Hunan (Grant No. 2021JJ20057); the Innovation Provincial Program of Hunan Province (Grant No. 2020RC3002). These financial supports are gratefully acknowledged.

Author contributions

Z.H. directed the program. W.D.X. and C.C.Z performed all the simulations. Z.H., W.D.X and Y.G.L. wrote the manuscript with the help and advice from W.D.W. and G.Q.C. N.S.C. and G.S.H. reviewed and edited the manuscript. All authors participated in data analysis, discussed the results and co-edited the manuscript. All authors participated in data analysis, discussed the results and co-edited the manuscript.

Competing interests

The authors declare no competing interests.

Data Availability Statement

The detailed information of the USGS flume experiment simulated in this study can be obtained at https://doi.org/10.1038/ngeo1040. The SPH implementation code used in this study can be obtained at https://github.com/DualSPHysics. The modeling parameters of this study can be obtained at https://doi.org/10.3390/W14091352. The experimental data used to validate the proposed model in this study can be obtained at https://github.com/dreamer0501/The-validation-data.

References

Arai, M., Huebl, J., & Kaitna, R. (2013), Occurrence conditions of roll waves for three grain-fluid models and comparison with results from experiments and field observation.

Geophysical Journal International, *195*(3), 1464-1480. https://doi.org/10.1093/gji/ggt352
Arattano, M., & Marchi, L. (2005), Measurements of debris flow velocity through cross-correlation of instrumentation data. *Natural Hazards and Earth System Science*, *5*(1), 137-142. https://doi.org/10.5194/nhess-5-137-2005
Chen, H., Hu, K., Cui, P., & Chen, X. (2017), Investigation of vertical velocity distribution in debris flows by PIV measurement. *Geomatics, Natural Hazards and Risk*, *8*(2), 1631-1642. https://doi.org/10.1080/19475705.2017.1366955
Chen, H.X., Li, J., Feng, S.J., Gao, H.Y., & Zhang, D.M. (2019), Simulation of interactions between debris flow and check dams on three-dimensional terrain. *Engineering Geology*, *251*, 48-62. https://doi.org/10.1016/j.enggeo.2019.02.001
Dowling, C.A., & Santi, P.M. (2014), Debris flows and their toll on human life: A global analysis of debris-flow fatalities from 1950 to 2011. *Natural Hazards*, *71*(1), 203-227. https://doi.org/10.1007/S11069-013-0907-4
Du, C., Wu, W.M., & Ma, C. (2021), Velocity profile of debris flow based on quadratic rheology model. *Journal of Mountain Science*, 18(8), 2120-2129. https://doi.org/10.1007/s11629-021-6790-7
Egashira, S., Ashida, K., Yajima, H., & Takahama, J. (1989), Constitutive equation of debris flow. *Annuals Disaster Prevention Research Institute, Kyoto University*, *32*(2), 487–501.
Gabriele, A., Tsoligkas, A.N., Kings, I.N., & Simmons, M.J.H. (2011), Use of PIV to measure turbulence modulation in a high throughput stirred vessel with the addition of high Stokes number particles for both up- and down-pumping configurations. *Chemical Engineering Science*, 66(23), 5862-5874. https://doi.org/10.1016/j.ces.2011.08.007
Godt, J.W. & Coe, J.A. (2007), Alpine debris flows triggered by a 28 July 1999 thunderstorm in the central Front Range, Colorado. *Geomorphology*, *84*(1-2), 80-97. https://doi.org/10.1016/j.geomorph.2006.07.009
Han, Z., Chen, G., Li, Y., Wang, W., & Zhang, H. (2015a), Exploring the velocity distribution of debris flows: An iteration algorithm based approach for complex cross-sections. *Geomorphology*, *241*, 72-82. https://doi.org/10.1016/j.geomorph.2015.03.043
Han, Z., Chen, G., Li, Y., Tang, C., Xu, L., He, Y., Huang, X., & Wang, W. (2015b), Numerical simulation of debris-flow behavior incorporating a dynamic method for estimating the entrainment. *Engineering Geology*, *190*, 52-64. https://doi.org/10.1016/j.enggeo.2015.02.009
Han, Z., Chen, G., Li, Y., & He, Y. (2015c), Assessing entrainment of bed material in a debris-flow event: A theoretical approach incorporating Monte Carlo method. *Earth Surface Processes and Landforms*, *40*(14), 1877-1890. https://doi.org/10.1002/esp.3766
Han, Z., Chen, G., Li, Y., Xu, L., Zheng, L., & Zhang, Y. (2014), A new approach for analyzing the velocity distribution of debris flows at typical cross-sections. *Natural Hazards*, *74*(3), 2053-2070. https://doi.org/10.1007/S11069-014-1276-3/FIGURES/14
Han, Z., Li, Y.G., Huang, J.L., Chen, G.Q., Xu, L.R., Tang, C., Zhang, H., & Shang, Y.H. (2017), Numerical simulation for run-out extent of debris flows using an improved cellular automaton model. *Bulletin of Engineering Geology and The Environment*, *76*(3), 961-974. https://doi.org/10.1007/s10064-016-0902-6
Han, Z., Su, B., Li, Y., Wang, Wei, Wang, Weidong, Huang, J., & Chen, G. (2019), Numerical simulation of debris-flow behavior based on the SPH method incorporating the Herschel-

Bulkley-Papanastasiou rheology model. *Engineering Geology*, *255*, 26-36. https://doi.org/10.1016/j.enggeo.2019.04.013
Han, Z., Wang, W., Li, Y., Huang, J., Su, B., Tang, C., Chen, G., & Qu, X. (2018), An integrated method for rapid estimation of the valley incision by debris flows. *Engineering Geology*, *232*, 34-45. https://doi.org/10.1016/j.enggeo.2017.11.007
Han, Z., Yang, F., Li, Y., Dou, J., Chen, N., Hu, G., Chen, G., & Xu, L. (2021a), GIS-Based Three-Dimensional SPH Simulation for the 11 April 2018 Yabakei Landslide at Oita Nakatsu, Japan. *Water*, *13*(21), 3012. https://doi.org/10.3390/W13213012
Han, Z., Zeng, C., & Li, Y. (2021b), Nonlinear vertical velocity distribution of debris flows using fluid-particle hierarchical statistical algorithm (in Chinese). *Journal of Engineering Geology*, 1-12. https://doi.org/10.13544/j.cnki.jeg.2021-0545
Han, Z., Zeng, C., & Li, Y. (2022), Hierarchical statistics-based nonlinear vertical velocity distribution of debris flow and its application in entrainment estimation. *Water*, *14*(9), 1352. https://doi.org/10.3390/W14091352
Hotta, N., Miyamoto, K., Suzuki, M., & Ohta, T. (1998), Pore-water pressure distribution of solid-water phase flow in a rolling mill. *Journal of the Japan Society of Erosion Control Engineering*, *50*(6), 11-16. https://doi.org/10.11475/sabo1973.50.6_11
Hotta, N., & Ohta, T. (2000), Pore-Water pressure of debris flows. *Physics and Chemistry of the Earth, Part B: Hydrology, Oceans and Atmosphere*, *25*(4), 381-385. https://doi.org/10.1016/S1464-1909(00)00030-7
Huang, G., Lv, G., Zhang, S., Huang, D., Zhao, L., Ni, X., Liu, H., Lv, J., & Liu, C. (2022). Numerical analysis of debris flows along the Sichuan-Tibet railway based on an improved 3D sphere DDA model and UAV-based photogrammetry. *Engineering Geology*, *305,* 106722. https://doi.org/10.1016/J.ENGGEO.2022.106722
Hungr, O., & McDougall, S. (2009). Two numerical models for landslide dynamic analysis. *Computers and Geosciences*, *35*(5), 978-992. https://doi.org/10.1016/j.cageo.2007.12.003
Iverson, R.M. (2012). Elementary theory of bed-sediment entrainment by debris flows and avalanches. *Journal of Geophysical Research: Earth Surface*, *117*(3), F03006. https://doi.org/10.1029/2011JF002189
Iverson, R.M. (1997). The physics of debris flows. *Reviews of Geophysics*, *35*(3), 245–296. https://doi.org/10.1029/97RG00426
Iverson, R.M., Reid, M.E., Logan, M., LaHusen, R.G., Godt, J.W., & Griswold, J.P. (2011). Positive feedback and momentum growth during debris-flow entrainment of wet bed sediment. *Nature Geoscience*, *4*(2), 116-121. https://doi.org/10.1038/ngeo1040
Iverson, R.M., & Vallance, J.W. (2001). New views of granular mass flows. *Geology, 29*(2), 115-118. https://doi.org/10.1130/0091-7613(2001)029<0115:NVOGMF>2.0.CO;2
Johnson, C.G., Kokelaar, B.P., Iverson, R.M., Logan, M., Lahusen, R.G., & Gray, J.M.N.T. (2012). Grain-size segregation and levee formation in geophysical mass flows. *Journal of Geophysical Research: Earth Surface*, *117*(1), F01032. https://doi.org/10.1029/2011JF002185
Liu, P., & Lam, K.M. (2015). Simultaneous PIV measurements of fluid and particle velocity fields of a sediment-laden buoyant jet. *Journal of Hydro-Environment Research*, *9*(2), 314-323. https://doi.org/10.1016/j.jher.2014.07.007

Luna, B. Q., Remaître, A., van Asch, T. W. J., Malet, J. P., & van Westen, C. J. (2012). Analysis of debris flow behavior with a one dimensional run-out model incorporating entrainment. *Engineering Geology*, *128*, 63-75. https://doi.org/10.1016/j.enggeo.2011.04.007

McDougall, S., & Hungr, O. (2005). Dynamic modelling of entrainment in rapid landslides. *Canadian Geotechnical Journal*, *42*(5), 1437-1448. https://doi.org/10.1139/t05-064

Morikawa, D.S., & Asai, M. (2022). A phase-change approach to landslide simulations: Coupling finite strain elastoplastic TLSPH with non-Newtonian IISPH. *Computers and Geotechnics*, *148,* 104815. https://doi.org/10.1016/J.COMPGEO.2022.104815

Nagl, G., Hübl, J., & Kaitna, R. (2020). Velocity profiles and basal stresses in natural debris flows. *Earth Surface Processes and Landforms*, *45*(8), 1764- https://doi.org/10.1002/esp.4844

Ouyang, C., He, S., & Tang, C. (2015). Numerical analysis of dynamics of debris flow over erodible beds in Wenchuan earthquake-induced area. *Engineering Geology*, *194*, 62-72. https://doi.org/10.1016/j.enggeo.2014.07.012

Prochaska, A.B., Santi, P.M., Higgins, J.D., & Cannon, S.H. (2008). A study of methods to estimate debris flow velocity. *Landslides, 5*(4), 431-444. https://doi.org/10.1007/s10346-008-0137-0

Pudasaini, S.P., & Fischer, J.T. (2020). A mechanical erosion model for two-phase mass flows. *International Journal of Multiphase Flow, 132,* 103416. https://doi.org/10.1016/j.ijmultiphaseflow.2020.103416

Remaître, A., W. J. Van Asch, T., Malet, J.P., & Maquaire, O. (2008). Influence of check dams on debris-flow run-out intensity. *Natural Hazards and Earth System Science*, *8*(6), 1403-1416. https://doi.org/10.5194/nhess-8-1403-2008

Rickenmann, D. (1999). Empirical relationships for debris flows. *Natural Hazards, 19*(1), 47-77. https://doi.org/10.1023/A:1008064220727

Takaoka, H., Hashimoto, H., Ikematsu, S., & Hikida, M. (2006). Prediction of landslide-induced debris flow hydrograph: The Atsumari debris flow disaster in Japan. *WIT Transactions on Ecology and the Environment*, *90*, 27-36. https://doi.org/10.2495/DEB060031

Takahashi, T. (2009). A review of Japanese debris flow research. *International journal of erosion control engineering*, *2*(1), 1–14.

Tang, C., Rengers, N., van Asch, T.W.J., Yang, Y.H., & Wang, G.F. (2011). Triggering conditions and depositional characteristics of a disastrous debris flow event in Zhouqu city, Gansu Province, northwestern China. *Natural Hazards and Earth System Science*, *11*(11), 2903-2912. https://doi.org/10.5194/nhess-11-2903-2011

Tecca, P.R., Deganutti, A.M., Genevois, R., & Galgaro, A. (2003). Velocity distributions in a coarse debris flow. *In: Chen, R. (Ed.), Debris-Flow Hazards Mitigation: Mechanics, Prediction, and Assessment Proceedings. Millpress, Rotterdam, The Netherlands* (pp, 905–916).

VanDine, D.F., & Bovis, M. (2002). History and goals of Canadian debris flow research, a review. *Natural Hazards, 26*(1), 69-82.

Wei, F., & Hu, K. (2009). Review and trends on debris flow velocity research (in Chinese). *Journal of Mountain Science*, *27*(5), 545–550.

Wei, F., Yang, H., Hu, K., & Chernomorets, S. (2012). Measuring internal velocity of debris flows by temporally correlated shear forces. *Journal of Earth Science*, *23*(3), 373-380. https://doi.org/10.1007/s12583-012-0258-1

Yu, D., Tang, L., & Chen, C. (2020). Three-dimensional numerical simulation of mud flow from a tailing dam failure across complex terrain. *Natural Hazards and Earth System Sciences*, *20*(3), 727-741. https://doi.org/10.5194/nhess-20-727-2020

Zanuttigh, B., & Lamberti, A. (2007). Instability and surge development in debris flows. *Reviews of Geophysics*, *45*(3), RG3006. https://doi.org/10.1029/2005RG000175

Journal of Geophysical Research-Earth Surface

Supporting Information for

Exploring the Temporal-Varying and Depth-Nonlinear Velocity Profile of Debris Flows Based on A Stratification Statistical Algorithm for 3D-HBP-SPH Particles

Zheng HAN[1,2], Wendou XIE[1], Chuicheng ZENG[1], Yange LI[1,3*], Changli LI[1], Haohui DING[1], Weidong WANG[1], Ningsheng CHEN[4], Guisheng HU[4], Guangqi CHEN[5]

[1] School of Civil Engineering, Central South University, Changsha 410075, China.

[2] Hunan Provincial Key Laboratory for Disaster Prevention and Mitigation of Rail Transit Engineering Structures, Changsha 410075, China.

[3] The Key Laboratory of Engineering Structures of Heavy Haul Railway, Ministry of Education, Changsha 410075, China.

[4] Key Lab of Mountain Hazards and Surface Processes, Institute of Mountain Hazards and Environment, Chinese Academy of Sciences, Chengdu 610041, China.

[5] Department of Civil Engineering, Kyushu University, Fukuoka, 819-0395, Japan.

Corresponding author: Y. Li (liyange@csu.edu.cn), No.22 Shaoshan South Road, School of Civil Engineering, Central South University, Changsha, Hunan, China. Tel.: +86 18684982076.

Contents of this file

Text S1. The 3D-HBP-SPH numerical model of debris flow

To supplement the 3D-HBP-SPH numerical model of debris flow described in the main text, we briefly review the basics of this model here.

The 3D-HBP-SPH model refers to a numerical model used to describe the dynamic process of debris flow. The main feature of this model is that under the Lagrange form, the three-dimensional smooth particle hydrodynamics (3D-SPH) calculation framework is integrated with the Herschel-Bulkley-Papanastasiou (HBP) rheological model of debris flow. It is well known that in the 3D-SPH method, debris flow and other fluids are regarded as continuous incompressible fluids, characterized by a group of discrete particles, whose behavior can be described by solving the Navier-Stokes equation, which can provide a solution to obtain velocity fields in three dimensions. In addition, the HBP rheological model can more comprehensively reflect the possible nonlinear rheological characteristics of debris flow slurry under large deformation. Moreover, the HBP rheological model has better convergence than the Bingham model.

Therefore, the 3D-HBP-SPH model combining the above two advantages can effectively describe the dynamic process of debris flow under various complex conditions, our previous study (Han et al., 2019) has shown that the 3D-HBP-SPH model has good applicability in the analysis of the dynamic process of debris flow.

The HBP rheological model is expressed as follows:

$$\boldsymbol{\tau}^{\boldsymbol{\alpha\beta}} = 2\mu_{eff}\boldsymbol{\varepsilon}^{\boldsymbol{\alpha\beta}} \tag{1}$$

$$\boldsymbol{\varepsilon}^{\boldsymbol{\alpha\beta}} = \frac{\mathbf{1}}{\mathbf{2}}\left(\frac{\partial \boldsymbol{v}^{\boldsymbol{\alpha}}}{\partial \boldsymbol{x}^{\boldsymbol{\beta}}} + \frac{\partial \boldsymbol{v}^{\boldsymbol{\beta}}}{\partial \boldsymbol{x}^{\boldsymbol{\alpha}}}\right) \tag{2}$$

$$\mu_{eff} = 2^{n-1}\mu_B\dot{\gamma}^{n-1} + \frac{\tau_y}{2\dot{\gamma}}(1 - e^{-m\dot{\gamma}}) \tag{3}$$

$$\tau_y = coh + P\tan\varphi \tag{4}$$

Where, $\boldsymbol{\tau}^{\boldsymbol{\alpha\beta}}$ is the shear stress tensor, μ_{eff} is the equivalent viscosity coefficient, $\boldsymbol{\varepsilon}^{\boldsymbol{\alpha\beta}}$ is the local strain rate tensor, μ_B is the Bingham viscosity coefficient, m and n are the constant and power law index controlling the stress growth under different shear rates respectively, τ_y is the yield stress under the Mohr-Coulomb yield criterion, coh is the cohesive force of soil, φ is the Angle of internal friction, P represents normal stress, $\dot{\gamma}$ represents shear strain rate, which is defined as:

$$\dot{\gamma} = \frac{\sqrt{2}}{2}\boldsymbol{\varepsilon}^{\boldsymbol{\alpha\beta}} \tag{5}$$

In the Lagrange form, the Navier-Stokes equation composed of momentum conservation equation can be expressed as follows:

$$\frac{d\boldsymbol{v_i}^{\boldsymbol{\alpha}}}{dt} = -\sum_{j=1}^{N} m_j \left(\frac{P_i}{{\rho_i}^2} + \frac{P_j}{{\rho_j}^2}\right)\frac{\partial W_{ij}}{\partial {x_i}^{\alpha}} + \sum_{j=1}^{N} m_j \left(\frac{2\mu_{eff\,i}{\varepsilon_i}^{\alpha\beta}}{{\rho_i}^2} + \frac{2\mu_{eff\,j}{\varepsilon_j}^{\alpha\beta}}{{\rho_j}^2}\right)\frac{\partial W_{ij}}{\partial {x_i}^{\beta}} + \boldsymbol{g}^{\boldsymbol{\alpha}} \tag{6}$$

Where, W_{ij} represents the kernel function; $\boldsymbol{v_i}^{\boldsymbol{\alpha}}$ and $\boldsymbol{g}^{\boldsymbol{\alpha}}$ represent particle velocity and gravity, respectively.

Please refer to our previous study (Han et al., 2019) for more details.

Figures S1 to S34. Summary of fitting results for 34 sets of experimental data

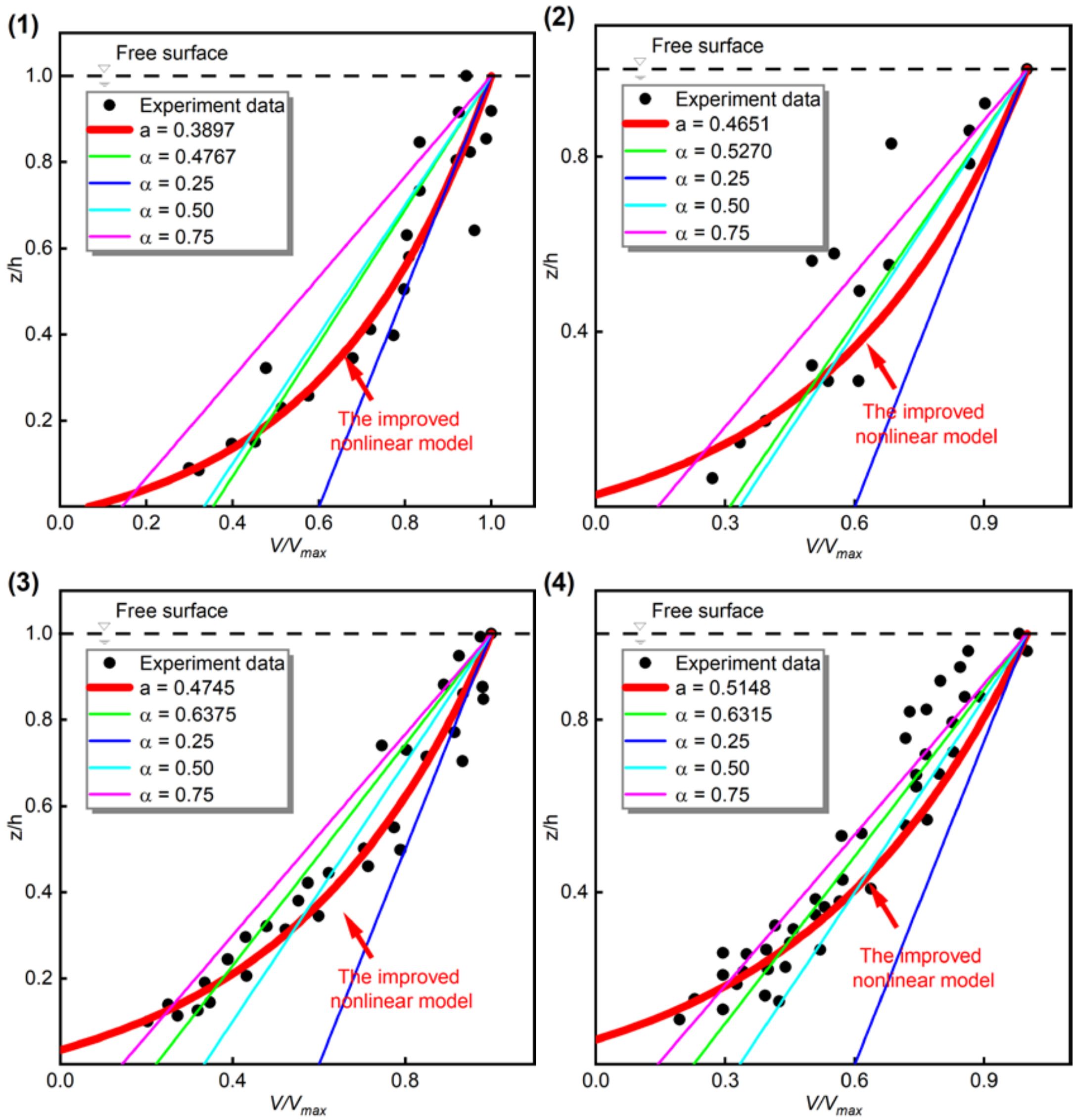

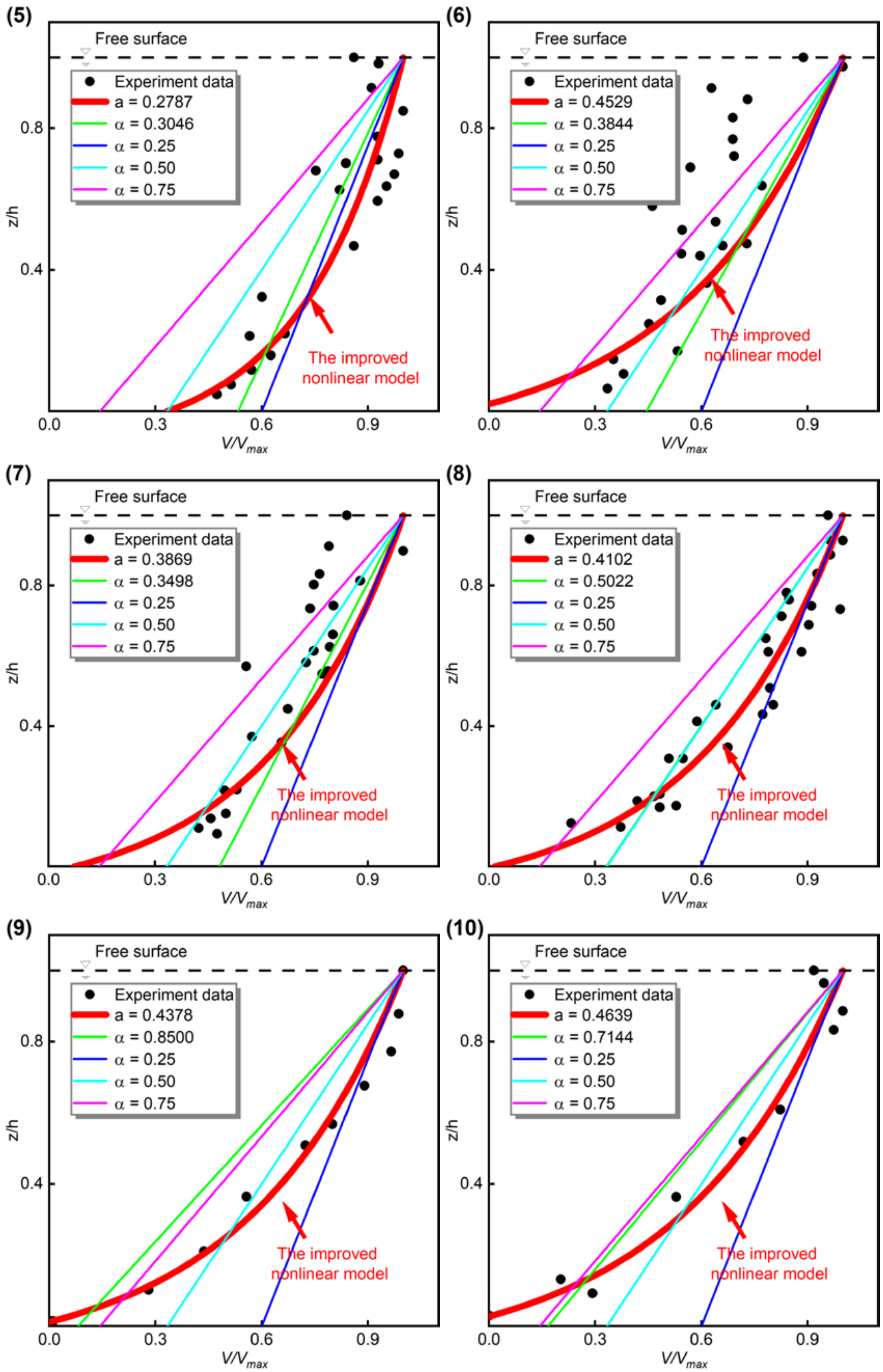
(5)
Free surface
Experiment data
a = 0.2787
α = 0.3046
α = 0.25
α = 0.50
α = 0.75
The improved nonlinear model
z/h
V/V_max
(6)
Free surface
Experiment data
a = 0.4529
α = 0.3844
α = 0.25
α = 0.50
α = 0.75
The improved nonlinear model
z/h
V/V_max
(7)
Free surface
Experiment data
a = 0.3869
α = 0.3498
α = 0.25
α = 0.50
α = 0.75
The improved nonlinear model
z/h
V/V_max
(8)
Free surface
Experiment data
a = 0.4102
α = 0.5022
α = 0.25
α = 0.50
α = 0.75
The improved nonlinear model
z/h
V/V_max
(9)
Free surface
Experiment data
a = 0.4378
α = 0.8500
α = 0.25
α = 0.50
α = 0.75
The improved nonlinear model
z/h
V/V_max
(10)
Free surface
Experiment data
a = 0.4639
α = 0.7144
α = 0.25
α = 0.50
α = 0.75
The improved nonlinear model
z/h
V/V_max

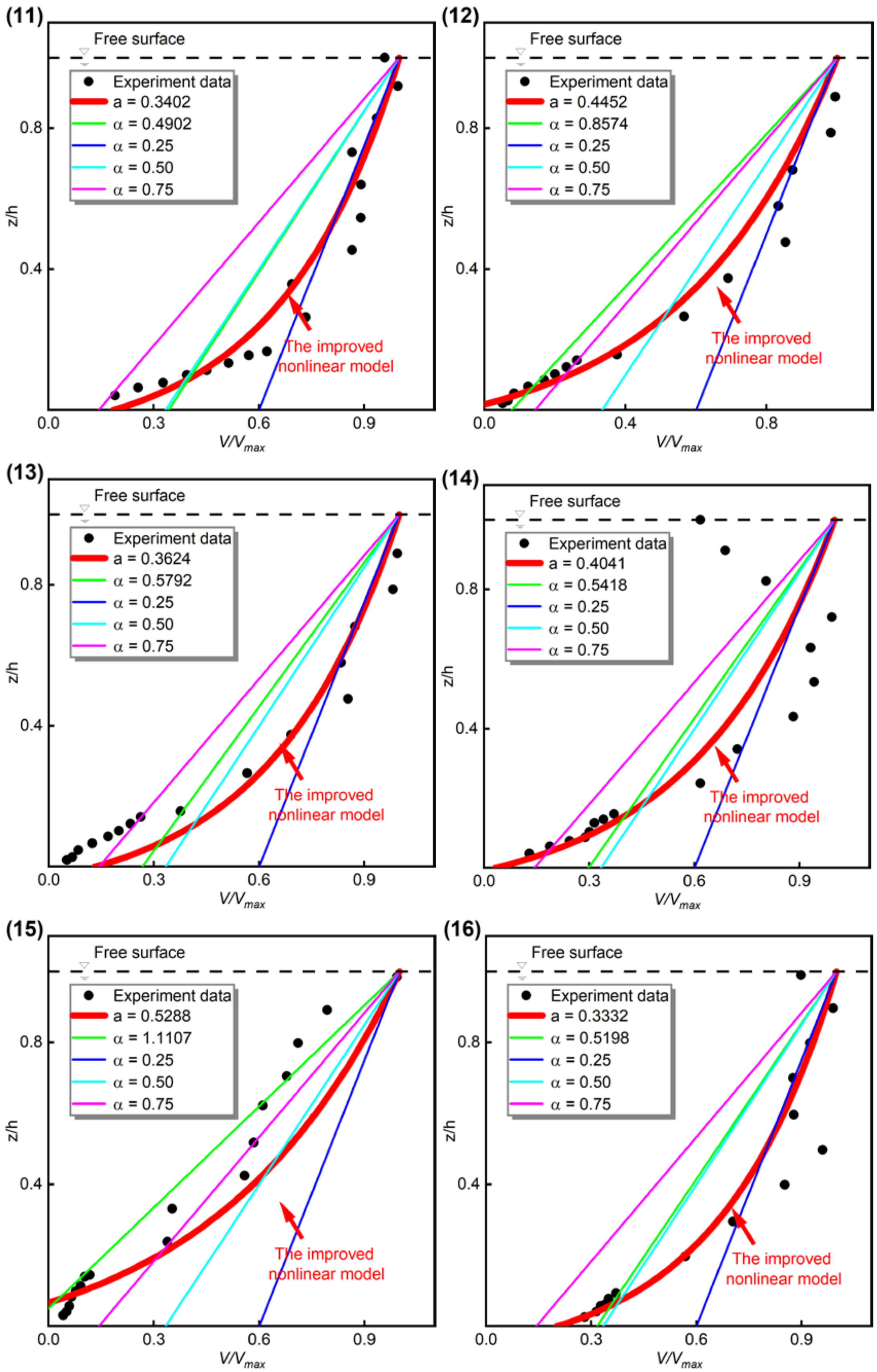

(11)
Free surface
Experiment data
a = 0.3402
α = 0.4902
α = 0.25
α = 0.50
α = 0.75
The improved nonlinear model
z/h
V/V_max
(12)
Free surface
Experiment data
a = 0.4452
α = 0.8574
α = 0.25
α = 0.50
α = 0.75
The improved nonlinear model
z/h
V/V_max
(13)
Free surface
Experiment data
a = 0.3624
α = 0.5792
α = 0.25
α = 0.50
α = 0.75
The improved nonlinear model
z/h
V/V_max
(14)
Free surface
Experiment data
a = 0.4041
α = 0.5418
α = 0.25
α = 0.50
α = 0.75
The improved nonlinear model
z/h
V/V_max
(15)
Free surface
Experiment data
a = 0.5288
α = 1.1107
α = 0.25
α = 0.50
α = 0.75
The improved nonlinear model
z/h
V/V_max
(16)
Free surface
Experiment data
a = 0.3332
α = 0.5198
α = 0.25
α = 0.50
α = 0.75
The improved nonlinear model
z/h
V/V_max

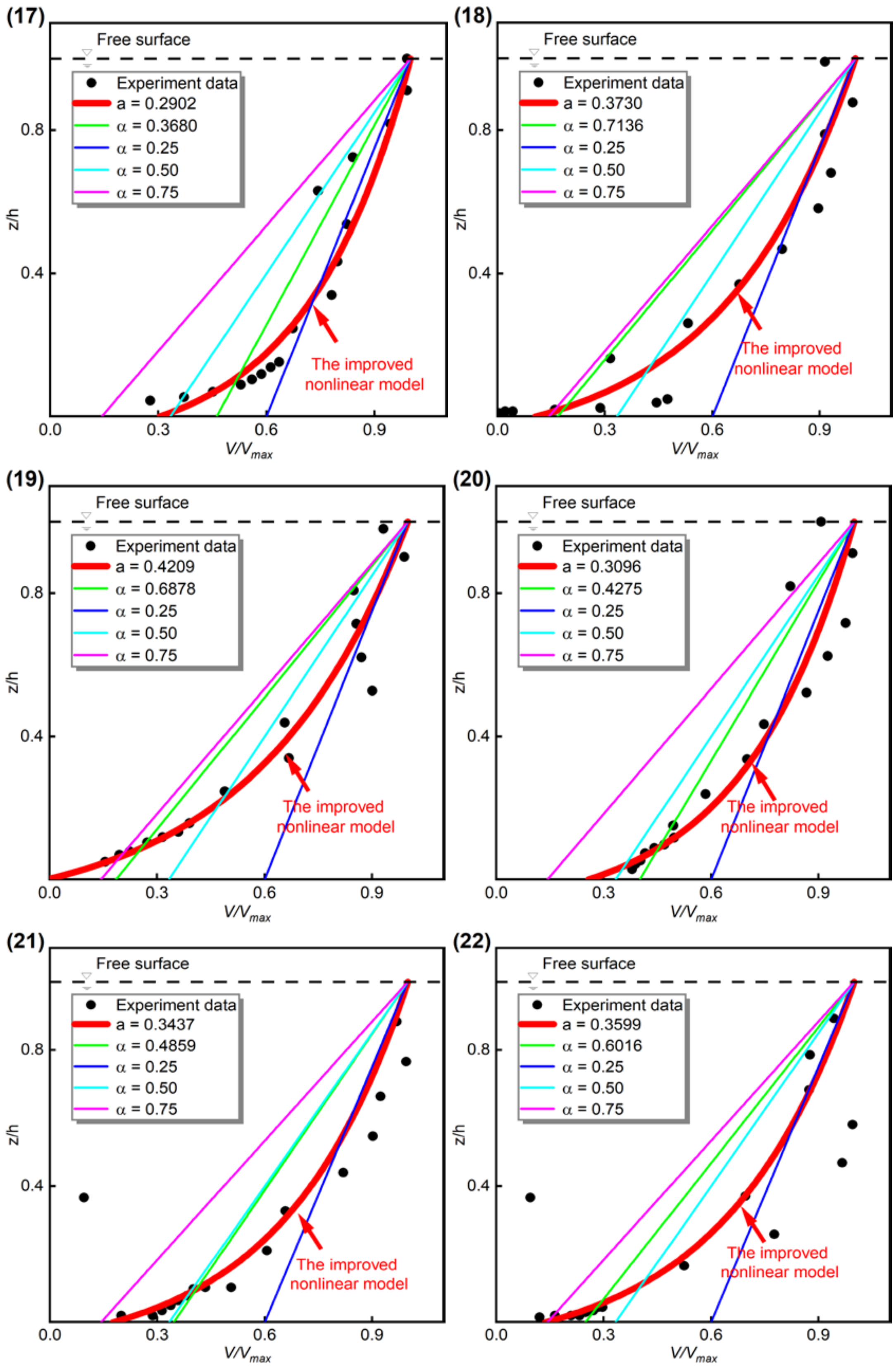
(17)
Free surface
Experiment data
a = 0.2902
α = 0.3680
α = 0.25
α = 0.50
α = 0.75
The improved nonlinear model
z/h
V/V_max
(18)
Free surface
Experiment data
a = 0.3730
α = 0.7136
α = 0.25
α = 0.50
α = 0.75
The improved nonlinear model
(19)
Free surface
Experiment data
a = 0.4209
α = 0.6878
α = 0.25
α = 0.50
α = 0.75
The improved nonlinear model
(20)
Free surface
Experiment data
a = 0.3096
α = 0.4275
α = 0.25
α = 0.50
α = 0.75
The improved nonlinear model
(21)
Free surface
Experiment data
a = 0.3437
α = 0.4859
α = 0.25
α = 0.50
α = 0.75
The improved nonlinear model
(22)
Free surface
Experiment data
a = 0.3599
α = 0.6016
α = 0.25
α = 0.50
α = 0.75
The improved nonlinear model

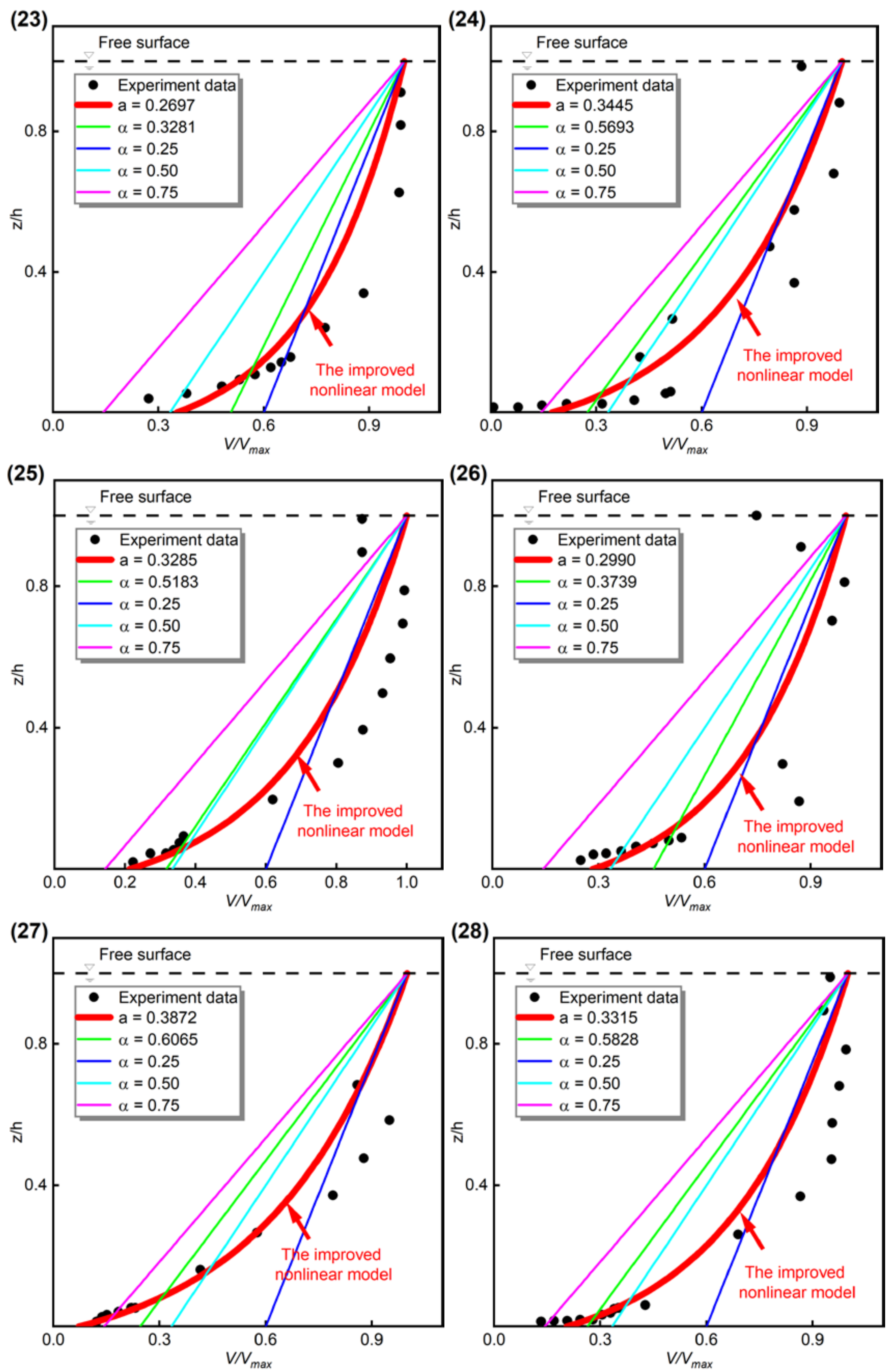
(23)
Free surface
Experiment data
a = 0.2697
α = 0.3281
α = 0.25
α = 0.50
α = 0.75
The improved nonlinear model
z/h
V/Vmax
(24)
Free surface
Experiment data
a = 0.3445
α = 0.5693
α = 0.25
α = 0.50
α = 0.75
The improved nonlinear model
z/h
V/Vmax
(25)
Free surface
Experiment data
a = 0.3285
α = 0.5183
α = 0.25
α = 0.50
α = 0.75
The improved nonlinear model
z/h
V/Vmax
(26)
Free surface
Experiment data
a = 0.2990
α = 0.3739
α = 0.25
α = 0.50
α = 0.75
The improved nonlinear model
z/h
V/Vmax
(27)
Free surface
Experiment data
a = 0.3872
α = 0.6065
α = 0.25
α = 0.50
α = 0.75
The improved nonlinear model
z/h
V/Vmax
(28)
Free surface
Experiment data
a = 0.3315
α = 0.5828
α = 0.25
α = 0.50
α = 0.75
The improved nonlinear model
z/h
V/Vmax

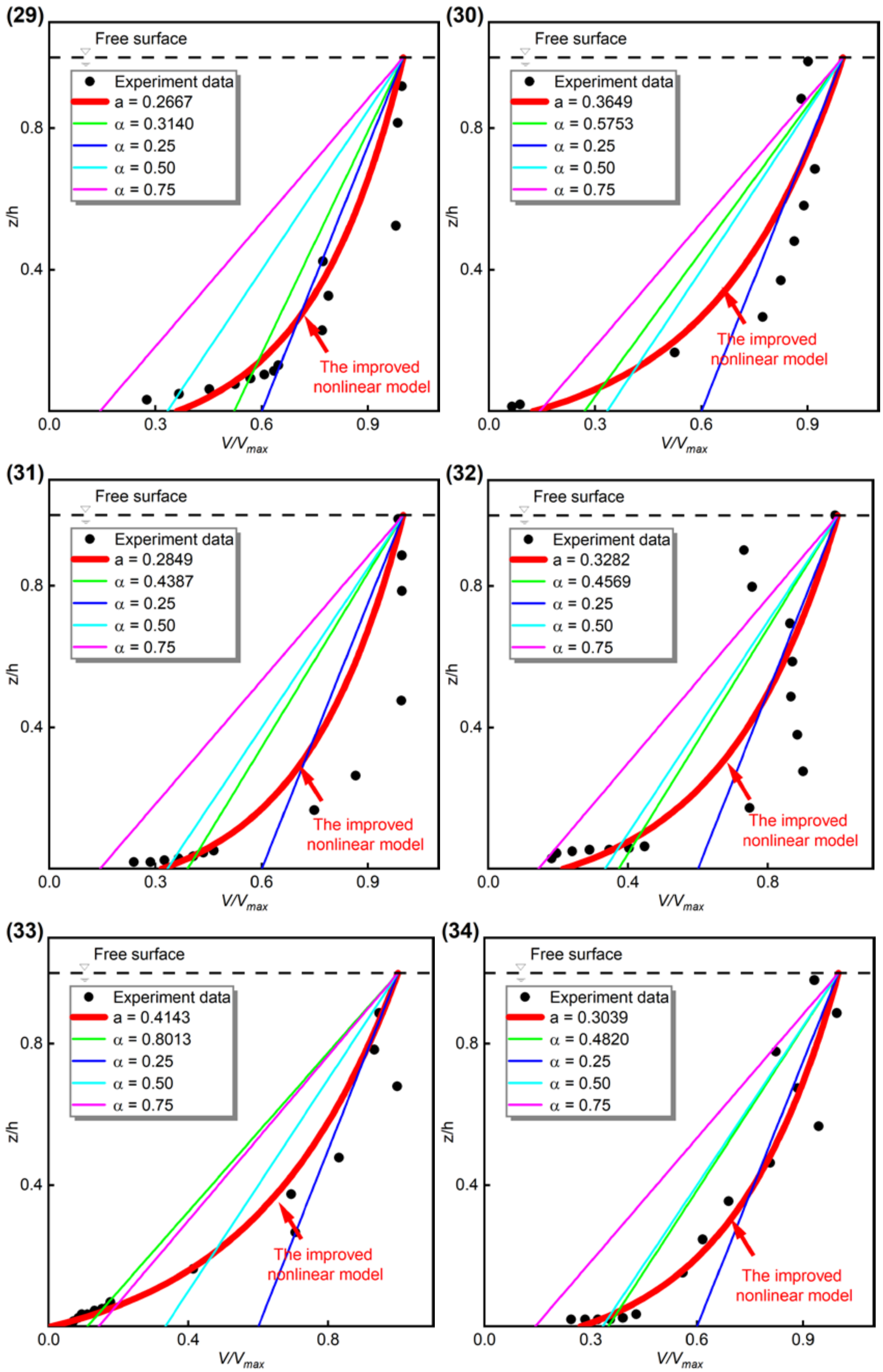

Figure S1 to S34. Summary of fitting results for 34 sets of experimental data.